# $I = 2\pi\pi$ scattering phase shift with two flavors of $O(a)$ improved dynamical quarks

T. Yamazaki,[1] S. Aoki,[1] M. Fukugita,[2] K-I. Ishikawa,[3] N. Ishizuka,[1,4] Y. Iwasaki,[1,4] K. Kanaya,[1] T. Kaneko,[5] Y. Kuramashi,[5] M. Okawa,[3] A. Ukawa,[1,4] and T. Yoshié[1,4]

(CP-PACS Collaboration)

[1]*Institute of Physics, University of Tsukuba, Tsukuba, Ibaraki 305-8571, Japan*
[2]*Institute for Cosmic Ray Research, University of Tokyo, Kashiwa, Chiba 277-8582, Japan*
[3]*Department of Physics, Hisoshima University, Higashi-Hiroshima, Hiroshima 739-8526, Japan*
[4]*Center for Computational Physics, University of Tsukuba, Tsukuba, Ibaraki 305-8577, Japan*
[5]*High Energy Accelerator Research Organization (KEK), Tsukuba, Ibaraki 305-0801, Japan*
(Received 23 February 2004; published 29 October 2004)

We present a lattice QCD calculation of phase shift including the chiral and continuum extrapolations in two-flavor QCD. The calculation is carried out for $I = 2$ $S$-wave $\pi\pi$ scattering. The phase shift is evaluated for two momentum systems, the center of mass and laboratory systems, by using the finite-volume method proposed by Lüscher in the center of mass system and its extension to general systems by Rummukainen and Gottlieb. The measurements are made at three different bare couplings $\beta = 1.80$, 1.95 and 2.10 using a renormalization group improved gauge and a tadpole improved clover fermion action, and employing a set of configurations generated for hadron spectroscopy in our previous work. The illustrative values we obtain for the phase shift in the continuum limit are $\delta(\deg.) = -3.50(64)$, $-9.5(30)$ and $-16.9(64)$ for $\sqrt{s}(\text{GeV}) = 0.4$, 0.6 and 0.8, which are consistent with experiments.

## I. INTRODUCTION

Calculation of scattering phase shift is an important step in expanding our understanding of the strong interaction based on lattice QCD beyond the hadron mass spectrum. For scattering lengths, which are the threshold values of phase shifts, several studies have already been carried out. For the simplest case of the two-pion system, $I = 2$ $S$-wave scattering length has been calculated in detail [1–8] including the continuum extrapolation [6,7]. There is also a pioneering attempt at $I = 0$ scattering length [3], which is much more difficult due to the presence of contributions from disconnected diagrams.

The first pioneering study of $I = 2$ $S$-wave scattering phase shift was made by Fiebig *et al.* [9]. They estimated the phase shift from the two-pion effective potential calculated in the lattice simulations. A direct calculation of phase shift on the lattice without recourse to effective potentials is possible if one uses the finite-volume method proposed by Lüscher [10,11]. In this method phase shift is obtained from the two-pion energy eigenvalues for finite volume. However, it is nontrivial to extract the energy eigenvalues from the time behavior of the two-pion correlation functions, because the correlation functions have multiexponential time behaviors due to presence of multiple states with the same quantum numbers. Recently we presented a direct calculation of the phase shift [8] in quenched QCD. In this calculation the diagonalization method proposed by Lüscher and Wolff [12] was used to solve the problem of the multiexponential behavior. Very recently Kim reported on his preliminary results

on $G$- and $H$-period boundary lattices, where the problem can be avoided by the boundary condition [13].

All previous studies of the scattering phase shift calculations were carried out with quenched approximation nor the continuum limit was taken. It is predicted in chiral perturbation theory that unphysical chiral divergences appear in the scattering length in the quenched theory due to the lack of unitarity [14,15]. The unphysical divergences can also occur in the phase shift. While the presence of such pathologies has not been numerically confirmed in actual lattice calculations with quenched approximation, we should make our study in full QCD in order to avoid such uncontrollable quenching problems.

In this paper we present a calculation of the physical scattering phase shift for $I = 2$ $S$-wave two-pion system including the dynamical quark effects and taking the continuum limit. We use the full QCD configurations previously generated for a study of light hadron spectrum [16] with a renormalization group improved gauge action and clover fermion action with a tadpole improved clover coefficient. We employ three lattice spacings corresponding to $a \approx 0.2$, 0.15 and 0.1 fm, and four pion masses in a region $m_\pi \approx 0.5 - 1.1$ GeV for each lattice spacing. The phase shift is evaluated by the finite-volume method as in the previous work [8]. In order to obtain the phase shift at several energies from one full QCD configuration, the calculations are carried out for two types of momentum systems. One of them is the center of mass system, where the total momentum of the two-pion system is zero. In the other system where the total momentum is fixed to a nonzero value, we use the method proposed by

Rummukainen and Gottlieb [17] which is a simple extension of that by Lüscher in the center of mass system to general momentum systems. We shall refer to this system as laboratory system in this paper.

This paper is organized as follows. In Sec. II we describe the finite-volume method for both momentum systems for evaluating the phase shift from the two-pion energy. We also explain the diagonalization method to extract the two-pion energy eigenvalues. The parameters of the calculation in this work are given in Sec. III . In Sec. IV we show data for the pion four-point functions and the effect of diagonalizations for the two momentum systems. We then present the results of the scattering length and the phase shift at each $\beta$ and in the continuum limit. In Sec. V we briefly summarize this work.

## II. METHODS

### A. Finite-volume method

#### 1. Center of mass system

In the center of mass system the total momentum of the two-pion system is zero. The energy eigenvalue of two pions in a finite periodic box $L^3$ without two-pion interactions is given by

$$E_n = 2\sqrt{m_\pi^2 + p_n^2}, \ \ p_n^2 = (2\pi/L)^2 n, \ \ n \in Z. \quad (1)$$

In the interacting case the total momentum is also zero and the energy eigenvalue of the $n$th state is given by

$$\overline{E}_n = 2\sqrt{m_\pi^2 + \overline{p}_n^2}, \ \ \overline{p}_n^2 = (2\pi/L)^2 \overline{n}, \ \ \overline{n} \not\in Z. \quad (2)$$

The energy eigenvalue is written as that of the free two-pion case with momentum $\overline{\mathbf{p}}_n$ and $-\overline{\mathbf{p}}_n$, but the quantity $\overline{n} = (L/2\pi)^2 \cdot \overline{p}_n^2$ is no longer an integer. Lüscher [10,11] found that the momentum $\overline{p}_n$ satisfies the relation

$$\tan\delta(\overline{p}_n) = \frac{\pi^{3/2}\sqrt{\overline{n}}}{Z_{00}(1;\overline{n})}, \quad (3)$$

where $\delta(\overline{p}_n)$ is the $S$-wave scattering phase shift in the infinite volume and

$$Z_{00}(s;\overline{n}) = \frac{1}{\sqrt{4\pi}} \sum_{\mathbf{n} \in Z^3} (n^2 - \overline{n})^{-s}. \quad (4)$$

The calculation method of $Z_{00}(s;\overline{n})$ is discussed in Appendix A. Using Eq. (3), we can obtain the phase shift from the energy eigenvalue calculated in the lattice simulations.

#### 2. Laboratory system

Let us consider a two-pion system with a nonzero total momentum $\mathbf{P} \neq 0$ in a periodic box $L^3$. We shall refer to this system as the laboratory system in the following. In the laboratory system the energy eigenvalue for the $n$th energy state $E_n^{\mathbf{P}}$ without interaction is given by

$$E_n^{\mathbf{P}} = \sqrt{m_\pi^2 + (p_{1,n}^{\mathbf{P}})^2} + \sqrt{m_\pi^2 + (p_{2,n}^{\mathbf{P}})^2},$$
$$L/(2\pi)\mathbf{p}_{1,n}^{\mathbf{P}} \in Z^3, \qquad L/(2\pi)\mathbf{p}_{2,n}^{\mathbf{P}} \in Z^3, \quad (5)$$

where $\mathbf{p}_{i,n}^{\mathbf{P}}$ is the $i$th pion momentum of the $n$th energy state in the laboratory system, which takes discrete values due to the periodic boundary condition in finite-volume. The two-pion interaction shifts $E_n^{\mathbf{P}}$ to $\overline{E}_n^{\mathbf{P}}$ as in the center of mass system. By the Lorentz transformation with a boost factor

$$\gamma = \overline{E}_n^{\mathbf{P}}/\sqrt{(\overline{E}_n^{\mathbf{P}})^2 - \mathbf{P}^2}, \quad (6)$$

the energy in the center of mass system can be obtained as

$$\overline{E}_n = \overline{E}_n^{\mathbf{P}}/\gamma. \quad (7)$$

It is noted that the total momentum $\mathbf{P}$ is not shifted by the two-pion interaction.

The center of mass momentum $\overline{p}_n$ is determined from $\overline{E}_n$ by

$$\overline{E}_n = 2\sqrt{m_\pi^2 + \overline{p}_n^2}, \qquad \overline{p}_n^2 = (2\pi/L)^2 \overline{m}, \qquad \overline{m} \not\in Z, \quad (8)$$

where $\overline{m}$ is also not an integer. Rummukainen and Gottlieb [17] found that the momentum $\overline{p}_n$ is related to the phase shift in the infinite volume through the relation

$$\tan\delta(\overline{p}_n) = \frac{\gamma\pi^{3/2}\sqrt{\overline{m}}}{Z_{00}^{\mathbf{d}}(1;\overline{m})}, \quad (9)$$

where

$$Z_{00}^{\mathbf{d}}(s;\overline{m}) = \frac{1}{\sqrt{4\pi}} \sum_{\mathbf{r} \in P^{\mathbf{d}}} (r^2 - \overline{m})^{-s}. \quad (10)$$

The summation for $\mathbf{r}$ is carried out over the set

$$P^{\mathbf{d}} = \{\mathbf{r}|\mathbf{r} = \hat{\gamma}^{-1}(\mathbf{n} + \mathbf{d}/2), \mathbf{n} \in Z^3\} \quad (11)$$

where $\mathbf{d} = L/(2\pi)\mathbf{P}$. The operation $\hat{\gamma}^{-1}$ is the inverse Lorentz transformation: $\hat{\gamma}^{-1}\mathbf{n} = 1/\gamma \cdot \mathbf{n}_{||} + \mathbf{n}_\perp$ , where $\mathbf{n}_{||} = (\mathbf{n} \cdot \mathbf{d})\mathbf{d}/d^2$ is the parallel component and $\mathbf{n}_\perp = \mathbf{n} - \mathbf{n}_{||}$ the perpendicular component of $\mathbf{n}$ in the direction $\mathbf{d}$. The calculation method of $Z_{00}^{\mathbf{d}}(s;\overline{m})$ is discussed in Appendix A. Substituting $\mathbf{d} = \mathbf{0}$ and $\gamma = 1$ into Eq. (9), we obtain the formula for the center of mass system Eq. (3).

### B. Extraction of energy eigenvalues of the two-pion system

In order to extract the two-pion energy eigenvalues in the system with a total momentum $\mathbf{P}$, we construct the pion four-point function by

$$G_{nm}^{(N_R)}(t) = \langle 0|\Omega_n(t)\Omega_m^{(N_R)}(t_S)|0\rangle, \quad (12)$$

where we omit the index for the total momentum. The

operator $\Omega_n(t)$ is a two-pion operator at time $t$ for the $n$th energy eigenstate which is defined by

$$\Omega_n(t) = \sum_{\mathbf{p}_1, \mathbf{p}_2 \in S_n} \pi(\mathbf{p}_1, t)\pi(\mathbf{p}_2, t)/[\sum_{\mathbf{p}_1, \mathbf{p}_2 \in S_n} 1], \quad (13)$$

where $\pi(\mathbf{p}, t)$ is the pion operator at time $t$ with momentum $\mathbf{p}$. The $\mathbf{p}_1$ and $\mathbf{p}_2$ are the momenta on the lattice and take discrete values, i.e., $L/(2\pi)\mathbf{p}_1 \in Z^3$, $L/(2\pi)\mathbf{p}_2 \in Z^3$. The summation for these momenta is taken over the set

$$S_n = \{\mathbf{p}_1, \mathbf{p}_2 | \sqrt{m_\pi^2 + \mathbf{p}_1^2} + \sqrt{m_\pi^2 + \mathbf{p}_2^2} \\ = E_n^{\mathbf{P}}, \mathbf{p}_1 + \mathbf{p}_2 = \mathbf{P}\}, \quad (14)$$

where $E_n^{\mathbf{P}}$ is fixed at the energy of the $n$th energy state with the total momentum $\mathbf{P}$ in the free two-pion case. This summation of momenta projects out the $A^+$ representation of the rotation group on the lattice, which equals the $S$-wave states in the continuum, ignoring the states with higher angular momentum. For example, states with angular momentum $l \geq 4$ are ignored for $L/(2\pi)\mathbf{P} = (0, 0, 0)$, and $l \geq 2$ for $L/(2\pi)\mathbf{P} = (1, 0, 0)$ and $(1, 1, 0)$.

For the source we use a different operator $\Omega_n^{(N_R)}(t)$ defined by

$$\Omega_n^{(N_R)}(t) = \frac{1}{N_R} \sum_{j=1}^{N_R} \pi(\mathbf{p}_{1,n}, t, \xi_j)\pi(\mathbf{p}_{2,n}, t, \eta_j), \quad (15)$$

where

$$\pi(\mathbf{p}, t, \xi_j)$$
$$= \frac{1}{L^3}\left[\sum_{\mathbf{x}} \overline{q}(\mathbf{x}, t)e^{i\mathbf{p}\cdot\mathbf{x}}\xi_j^\dagger(\mathbf{x})\right]\gamma_5\left[\sum_{\mathbf{y}} q(\mathbf{y}, t)\xi_j(\mathbf{y})\right]. \quad (16)$$

Here $\mathbf{p}_{1,n}, \mathbf{p}_{2,n}$ are fixed to one of the values in the set $S_n$ for the sink operator $\Omega_n(t)$ defined in Eq. (13). The functions $\xi_j(\mathbf{x})$ and $\eta_j(\mathbf{x})$ are complex random numbers in three-dimensional space, whose property is

$$\lim_{N_R \to \infty} \frac{1}{N_R} \sum_{j=1}^{N_R} \xi_j^\dagger(\mathbf{x})\xi_j(\mathbf{y}) = L^3\delta_{\mathbf{x}, \mathbf{y}}. \quad (17)$$

The pion propagator is also calculated with the random number as

$$G_n^{\pi(N_R)}(t) = \frac{1}{N_R} \sum_{j=1}^{N_R} \langle 0|\pi(\mathbf{p}_n, t)\pi(-\mathbf{p}_n, t_S, \xi_j)|0\rangle. \quad (18)$$

When the number of random noise sources $N_R$ is taken large or the number of gauge configurations is large, we expect

$$G_{nm}^{(N_R)}(t) \sim G_{nm}(t) = \langle 0|\Omega_n(t)\Omega_m(t_S)|0\rangle,$$
$$G_n^{\pi(N_R)}(t) \sim G_n^\pi(t) = \langle 0|\pi(\mathbf{p}_n, t)\pi(-\mathbf{p}_n, t_S)|0\rangle, \quad (19)$$

and the four-point function will be symmetric under the

exchange of the sink and the source indices $n$ and $m$. We fix $N_R = 2$ in all calculations. The number of the gauge configurations is from 380 to 725 depending on the lattice spacing as shown in Sec. III.

The four-point function can be written in terms of the energy eigenstates $|\overline{\Omega}_n\rangle$ with the total momentum $\mathbf{P}$ as follows:

$$G_{nm}(t) = \sum_j V_{nj}^T V_{jm} e^{-\overline{E}_j^{\mathbf{P}}(t-t_S)}, \quad V_{jm} = \langle \overline{\Omega}_j|\Omega_m(0)|0\rangle,$$
$$(20)$$

where $\overline{E}_n^{\mathbf{P}}$ is the energy eigenvalues with the two-pion interaction. Since the matrix $V_{jm}$ is not diagonal generally, the four-point function contains many exponential terms and is not diagonal with respect to $n$ and $m$.

A simple method for extracting the energy eigenvalues is diagonalization of $G(t)$ at each $t$. Lüscher and Wolff [12] found that the eigenvalue is given by $\lambda_n(t) = \exp(-\overline{E}_n^{\mathbf{P}}t) \times \{1 + O(\exp[-\Delta_n t])\}$ with $\Delta_n = \min_{n \neq m}|\overline{E}_n^{\mathbf{P}} - \overline{E}_m^{\mathbf{P}}|$. In order to extract $\overline{E}_n^{\mathbf{P}}$ from the eigenvalue by a single exponential fit, we have to analyze $G(t)$ in the large $t$ region where $O(\exp[-\Delta_n t])$ terms can be neglected. However, it may be very difficult to employ the fitting with this method due to loss of statistics of $G(t)$ in the large $t$ region.

Lüscher and Wolff also proposed another method [12], which is a diagonalization of the matrix $M(t, t_0)$ constructed from $G(t)$ by

$$M(t, t_0) = G(t_0)^{-1/2}G(t)G(t_0)^{-1/2}, \quad (21)$$

where $t_0$ is a reference time. The eigenvalues of $M(t, t_0)$ equals

$$\lambda_n(t, t_0) = e^{-\overline{E}_n^{\mathbf{P}}(t-t_0)}, \quad (22)$$

without $O(\exp[-\Delta_n t])$ terms. Therefore after the diagonalization of $M(t, t_0)$ we can extract the two-pion energy eigenvalue by a single exponential fitting of $\lambda_n(t, t_0)$. In this work we adopt the second method.

In the diagonalization method we assume that the two-pion states dominate and effects from other states can be neglected in $G(t)$ for the considered range of $t$. For example, our analysis loses its validity when the center of mass two-pion energy is over the inelastic scattering limit, e.g., $\overline{E} \geq 4m_\pi$. In this case $G(t)$ is dominated by the four-pion ground state rather than the two-pion state in the large $t$ region. Further, we should pay attention to the states contained with the excited pion state, such as $\pi\pi^*(1300)$. The existence of such undesirable states is discussed in Sec. III.

Since we cannot calculate all components of $G(t)$ in the actual lattice calculations, a cut-off of the state $N$ has to be introduced. We expect that the components of $G_{nm}(t)$ with $n, m \leq k$ dominate for the $k$th eigenvalue $\lambda_k(t)$ in the large $t$ and $t_0$ region, while the components $n, m > k$ are

less important. We set $t$ and $t_0$ large and investigate the dependence for the cut-off $N \geq k$.

### III. PARAMETERS

We calculate the scattering phase shift on the gauge configurations previously generated including two flavors of dynamical quark effects for the study of the light hadron spectrum [16]. This work employed a renormalization group improved gauge action and clover fermion action with a tadpole improved clover coefficient $c_{SW}$, which we also use in the present study. The gauge action is constructed in terms of the $1 \times 1$ and $1 \times 2$ Wilson loops $W^{1 \times 1}$ and $W^{1 \times 2}$,

$$S_G = \frac{\beta}{6}\left[ c_0 \sum_{x,\mu<\nu} W^{1\times1}_{\mu\nu}(x) + c_1 \sum_{x,\mu,\nu} W^{1\times2}_{\mu\nu}(x) \right]. \quad (23)$$

The coefficient $c_1$ is fixed to $c_1 = -0.331$ by an approximate renormalization group analysis and $c_0 = 1 - 8c_1 = 3.648$ by the normalization condition [18]. The bare gauge coupling $\beta$ is defined by $\beta = 6/g^2$. For clover fermion action [19] a mean-field improved clover coefficient $c_{SW} = (W^{1\times1})^{-3/4}$ is adopted, where the plaquette $W^{1\times1} = 1 - 0.8412/\beta$ is determined by one-loop perturbation theory [18].

The parameters for the configuration generation are summarized in Table I. The configurations were generated at $\beta = 1.80$ and 1.95 and 2.10, and for four hopping parameters $\kappa$ corresponding to $m_\pi/m_\rho \approx 0.6 - 0.8$ in each $\beta$. The lattice spacing is estimated from the $\rho$ meson mass and equals $a = 0.2150(22)$, $0.1555(17)$ and $0.1076(13)$ fm, respectively. The lattice size $L^3 \times T$ at each $\beta$ is $12^3 \times 24$, $16^3 \times 32$ and $24^3 \times 48$, which correspond to a $2.5^3$ fm$^3$ lattice. The periodic boundary con-

ditions are imposed both in the spatial and time directions.

The quark propagators are calculated with the periodic boundary condition in the spatial directions, and the Dirichlet boundary condition in the temporal direction. The source operator $\Omega_n^{(N_R)}(t_S)$ is set at $t_S = 4$ for $\beta = 1.80$ and $\beta = 1.95$, and $t_S = 6$ for $\beta = 2.10$ to reduce effects from the temporal boundary. In order to avoid effects from excited states, the reference time for the diagonalization introduced in Eq. (21) is fixed to large value; $t_0 = 10$, 12 and 16 at $\beta = 1.80$, 1.95 and 2.10, respectively. At $\beta = 1.80$ for the lightest quark mass we carry out extra measurements to reduce statistical errors in which the source operator is located at $t_S + T/2$ and the Dirichlet boundary condition in the temporal direction is imposed at $T/2$. We average over the two measurements for the analysis of the pion four-point functions and the pion propagator.

In order to extract the phase shift at various momenta from a single full QCD configuration, the calculations are carried out in three momentum systems, the center of mass (CM) and two laboratory systems (L1 and L2), whose total momenta are

|   |   | $L/(2\pi)\mathbf{P}$ |   |
|---|---|---|---|
| CM | Center of mass system | $(0, 0, 0)$ | |
| L1 | Laboratory system | $(1, 0, 0)$ | (24) |
| L2 | Laboratory system | $(1, 1, 0)$. | |

In Table II we show the momenta chosen for the source operator $\Omega_n^{(N_R)}$ defined in Eq. (15). All elements in $S_n$, which appear in the summation over momenta in the sink operator $\Omega_n$ defined in Eq. (13), can be obtained from the source momenta by cubic, tetragonal and orthorhombic

TABLE I. Simulation parameters. The lattice spacing $a$ is fixed by the $\rho$ meson mass at the physical pion mass and $m_\rho = 768.4$ MeV. $N_{\mathrm{Traj}}$ is the number of all trajectories, $N_{Skip}$ is the number of separation between two measurements and $N_{\mathrm{Meas}}$ is the number of the configurations used the measurements.

| $\beta$ | $L^3 \times T$ | $c_{SW}$ | $a$ [fm] | $La$ [fm] | $\kappa$ | $m_\pi/m_\rho$ | $N_{\mathrm{Traj}}$ | $N_{\mathrm{Skip}}$ | $N_{\mathrm{Meas}}$ |
|---|---|---|---|---|---|---|---|---|---|
| 1.80 | $12^3 \times 24$ | 1.60 | 0.2150(22) | 2.580(26) | 0.1409 | 0.807(1) | 6530 | 10 | 645 |
|  |  |  |  |  | 0.1430 | 0.753(1) | 5240 | 10 | 520 |
|  |  |  |  |  | 0.1445 | 0.694(2) | 7350 | 10 | 725 |
|  |  |  |  |  | 0.1464 | 0.547(4) | 5250 | 10 | 405[a] |
| 1.95 | $16^3 \times 32$ | 1.53 | 0.1555(17) | 2.489(27) | 0.1375 | 0.804(1) | 7000 | 10 | 595 |
|  |  |  |  |  | 0.1390 | 0.752(1) | 7000 | 10 | 690 |
|  |  |  |  |  | 0.1400 | 0.690(1) | 7000 | 10 | 685 |
|  |  |  |  |  | 0.1410 | 0.582(3) | 5000 | 10 | 495 |
| 2.10 | $24^3 \times 48$ | 1.47 | 0.1076(13) | 2.583(31) | 0.1357 | 0.806(1) | 4000 | 10 | 395 |
|  |  |  |  |  | 0.1367 | 0.755(2) | 4000 | 10 | 390 |
|  |  |  |  |  | 0.1374 | 0.691(3) | 4000 | 10 | 380 |
|  |  |  |  |  | 0.1382 | 0.576(3) | 4000 | 5 | 640 |

[a]We average two measurements on the same configuration, one with the temporal origin located at $t = 0$ and the other located at $t = T/2$.

TABLE II.   Momentum assignment for the source operator $\Omega_n^{(N_R)}(t)$ defined by Eq. (15). Here $\mathbf{p}_{i,n}$ is the $i$th pion momentum of the $n$ state $\mathbf{P}$ is the total momentum of two pions system $\mathbf{P} = \mathbf{p}_{1,n} + \mathbf{p}_{2,n}$ in units of $2\pi/L$.

| CM $\mathbf{P} = (0, 0, 0)$ | $n = 0$ | $n = 1$ | $n = 2$ | $n = 3$ |
|---|---|---|---|---|
| $\mathbf{p}_{1,n}$ | $(0, 0, 0)$ | $(1, 0, 0)$ | $(1, 1, 0)$ | $(1, 1, 1)$ |
| $\mathbf{p}_{2,n}$ | $(0, 0, 0)$ | $(-1, 0, 0)$ | $(-1, -1, 0)$ | $(-1, -1, -1)$ |
| L1 $\mathbf{P} = (1, 0, 0)$ | $n = 0$ | $n = 1$ | $n = 2$ | $n = 3$ |
| $\mathbf{p}_{1,n}$ | $(1, 0, 0)$ | $(1, 1, 0)$ | $(2, 0, 0)$ | $(1, 1, 1)$ |
| $\mathbf{p}_{2,n}$ | $(0, 0, 0)$ | $(0, -1, 0)$ | $(-1, 0, 0)$ | $(0, -1, -1)$ |
| L2 $\mathbf{P} = (1, 1, 0)$ | $n = 0$ | $n = 1$ | $n = 2$ | $n = 3$ |
| $\mathbf{p}_{1,n}$ | $(1, 1, 0)$ | $(1, 0, 0)$ | $(1, 1, 1)$ | $(1, 0, 1)$ |
| $\mathbf{p}_{2,n}$ | $(0, 0, 0)$ | $(0, 1, 0)$ | $(0, 0, -1)$ | $(0, 1, -1)$ |

rotations on the lattice for the CM, L1 and L2 systems, respectively.

The center of mass energies of the free two-pion system $E_n$ in this work are plotted in Fig. 1, where the smallest pion mass at $\beta = 2.10$ is assumed. In all systems the phase shift is evaluated at the ground ($n = 0$) and first excited states ($n = 1$), which are denoted by closed symbols. Other higher energy states ($n \geq 2$) plotted by open symbols are used to investigate the effects of the cut-off $N$ introduced in the diagonalization. In the two laboratory systems, L1 and L2, we also calculate the $n = 3$ state, because the energies of these states are very close to the $n = 2$ state as shown in the figure and effects from these states can be comparable. We also plot the location of the

inelastic scattering threshold, $E \geq 4m_\pi$, and the energy of state $\pi\pi^*(1300)$, which can appear in the pion four-point function and causes loss of validity of the diagonalization method as discussed in Sec. II B. We neglect the quark mass dependence of $\pi^*(1300)$ in the estimation. As shown in Fig. 1 the energies of these undesirable states are very far from the measured point of the scattering phase shift.

We estimate the errors of the four-point functions and the pion propagator by the jackknife method. In our study of the light hadron spectrum [16], we have shown that the separation of 50 trajectories covers all the autocorrelations of the configuration, so that in the present analysis we also use bins of 50 trajectories in the jackknife method. In the actual analysis a bin size of five or ten ($\beta = 2.10$ at the lightest quark mass) measurements are employed, because we skip ten or five trajectories between successive measurements.

## IV. RESULTS

### A. Effect of diagonalization

In Fig. 2 we plot the absolute value of the pion four-point function $G_{nm}(t)$ defined by Eq. (12) at several values of $n$ and $m$ for the three momentum systems. This figure corresponds to $m_\pi/m_\rho \approx 0.6$ at $\beta = 2.10$. Filled and open symbols indicate positive and negative values. In all systems, the off-diagonal components of $G_{nm}(t)$ ($n \neq m$) are not negligible compared with the diagonal components ($n = m$). We also observe that the shape of $G_{nm}(t)$ in the CM and L1 systems are very similar. In the L2 system $G_{00}(t)$ is almost the same as $G_{11}(t)$ for all $t$. This is attributed to the fact that these energies are very close in the free two-pion case. The figure also shows that $G_{nm}(t)$ is symmetric under the exchange of the indices as expected. In the following analysis we assume the symmetry of $G_{nm}(t)$ and we average values of the symmetric components.

In order to investigate the effect of diagonalization we define two ratios $R_n(t)$ and $D_n(t)$ as follows,
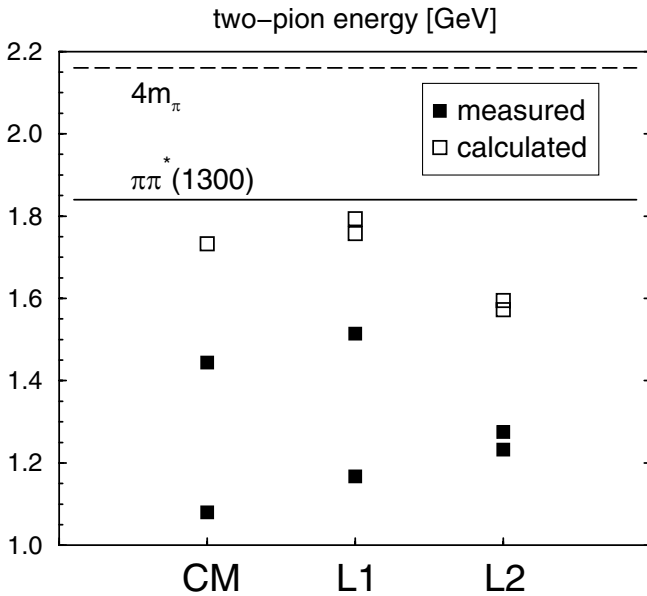


FIG. 1.   Center of mass energy of two-pion system for $m_\pi/m_\rho \approx 0.6$ at $\beta = 2.10$ without the two-pion interaction. We measure the scattering phase shifts at the energies referred by filled symbols. States denoted by open symbols are used only to examine the effect of the cut-off of the state for the diagonalization. Solid and dashed lines denote the $\pi\pi^*(1300)$ state energy and the inelastic scattering limit, respectively.
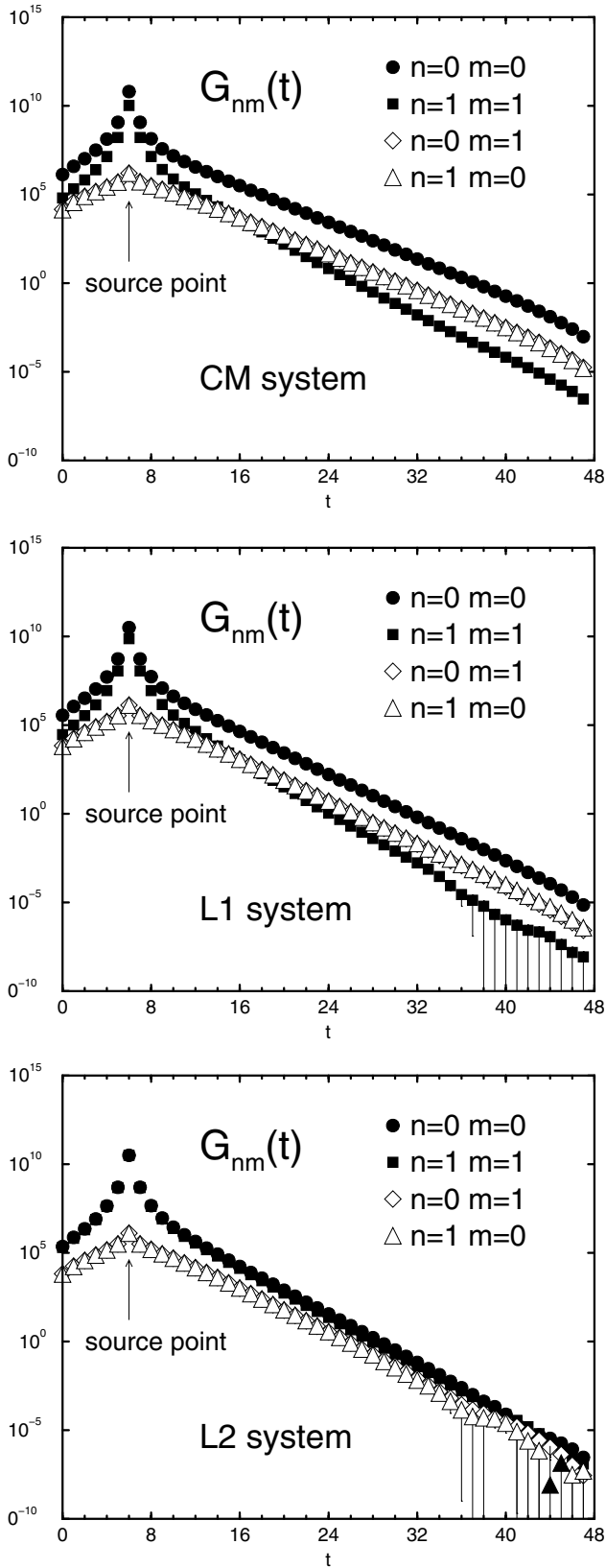
FIG. 2.   Examples of the pion four-point function $G_{nm}(t)$ in the center of mass system CM and two laboratory systems L1 and L2 for $m_\pi/m_\rho \approx 0.6$ at $\beta = 2.10$. Filled and open symbols indicate positive and negative value.

$$R_n(t) = \frac{G_{nn}(t)}{G_{1,n}^\pi(t)G_{2,n}^\pi(t)}, \tag{25}$$

$$D_n(t) = \lambda_n(t,t_0)\frac{G_{1,n}^\pi(t_0)G_{2,n}^\pi(t_0)}{G_{1,n}^\pi(t)G_{2,n}^\pi(t)}, \tag{26}$$

where $G_{i,n}^\pi(t)$ is the $i$th pion propagator for the $n$th energy state, and $\lambda_n(t,t_0)$ is the $n$th eigenvalue of the matrix $M(t,t_0)$ defined by Eq. (21) calculated with a finite cut-off of the energy state $N$. If the pion four-point function contains only a single exponential term, i.e., $G_{nm}(t) \propto \delta_{nm}\cdot\exp[-\overline{E}_n^{\mathbf{P}}(t-t_S)]$, then the ratio $R_n(t)$ behaves as

$$R_n(t) = A\cdot\exp[-\Delta\overline{E}_n^{\mathbf{P}}(t-t_S)], \tag{27}$$

where $\Delta\overline{E}_n^{\mathbf{P}} = \overline{E}_n^{\mathbf{P}} - E_n^{\mathbf{P}}$ and $A$ is a constant. If the cut-off of the state $N$ for the diagonalization is sufficiently large, then the ratio $D_n(t)$ behaves as

$$D_n(t) = \exp[-\Delta\overline{E}_n^{\mathbf{P}}(t-t_0)]. \tag{28}$$

In these cases we can extract the $n$th energy shift $\Delta\overline{E}_n^{\mathbf{P}}$ from the ratios $R_n(t)$ or $D_n(t)$ by a single exponential fitting.

First we focus on the results in the CM system. For the ground state ($n = 0$) the ratios $R_0(t)$ and $D_0(t)$ for all $m_\pi/m_\rho$ and $\beta$ are presented in Fig. 3. We divide the ratio $D_0(t)$ by $D_0(t_S)$ for comparison with $R_0(t)$. The cut-off of the state $N$ for the diagonalization is set at $N = 2$. We also check the cut-off dependence by taking $N = 1$ and confirm that it is negligible. From the figures we find that the diagonalization does not affect the result of the ground state and the energy shift can be extracted from the ratio $R_0(t)$ without the diagonalization.

We compare the ratios for the first excited state ($n = 1$) in the CM system in Fig. 4, where the cut-off is set at $N = 1$ and 2. Here we divide $D_1(t)$ by $D_1(t_S)$ as for $n = 0$. In contrast to the case of the ground state the diagonalization is very effective for the smaller quark masses. The ratio $R_1(t)$ for smaller masses rapidly increases, while such behavior cannot be seen in $D_1(t)$. The cut-off dependence of $D_1(t)$ is negligible for whole parameter regions as shown in the figure. Hence we can extract the energy shift from the ratio $D_1(t)$ by a single exponential fitting.

The ratios in the L1 system are plotted in Fig. 5 for the ground state ($n = 0$); we also divide $D_n(t)$ by $D_n(t_S)$ as for the CM system. We find that $R_0(t)$ agrees with $D_0(t)$ with $N = 3$. We also check the cut-off dependence by taking $N = 1, 2$ and confirm that it is negligible. This indicates that the energy shift can be extracted without the diagonalization as for the ground state in the CM system. For the first excited state ($n = 1$), however, the diagonalization is effective as shown in Fig. 6. We also find that the effect of the cut-off for $D_1(t)$ is negligible by comparing the results with $N = 1, 2$   and   3. The ratio $D_1(t)$ at $\beta =$
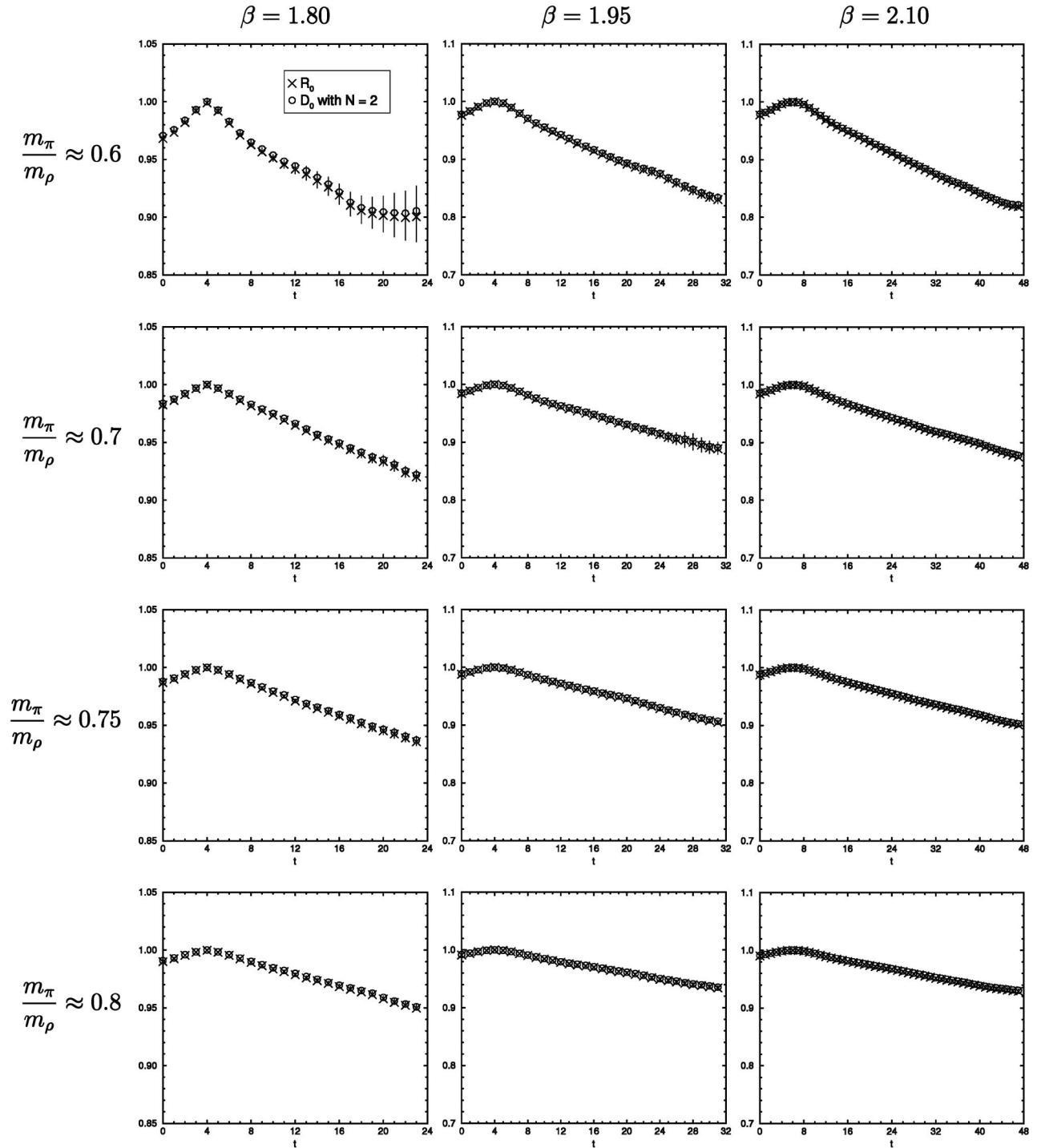
FIG. 3.    Ratios $R_n(t)$ and $D_n(t)$ for $n = 0$ in the center of mass system CM with energy state cut-off $N = 2$. $m_\pi/m_\rho$ increases from top to bottom, while $\beta$ increases from left to right.

1.95 and 2.10 for $m_\pi/m_\rho \approx 0.6$ do not show good exponential behaviors. We consider that this is due to insufficient statistics and do not include these data in the following analysis.

Finally we focus on the L2 system. The behavior of the ratios in this system is essentially different from those in the other systems. The ratios $R_n(t)$ and

$D_n(t)$ are shown in Fig. 7 for the ground ($n = 0$) and in Fig. 8 for the first excited states ($n = 1$). In these figures $D_n(t)$ is divided by $D_n(t_S)$. Since the energies of $n = 0$ and one states are very close in the free two-pion case, not only the ratio for $n = 1$ but also that for $n = 0$ are affected by the diagonalization. We also observe that the cut-off dependence is negligible
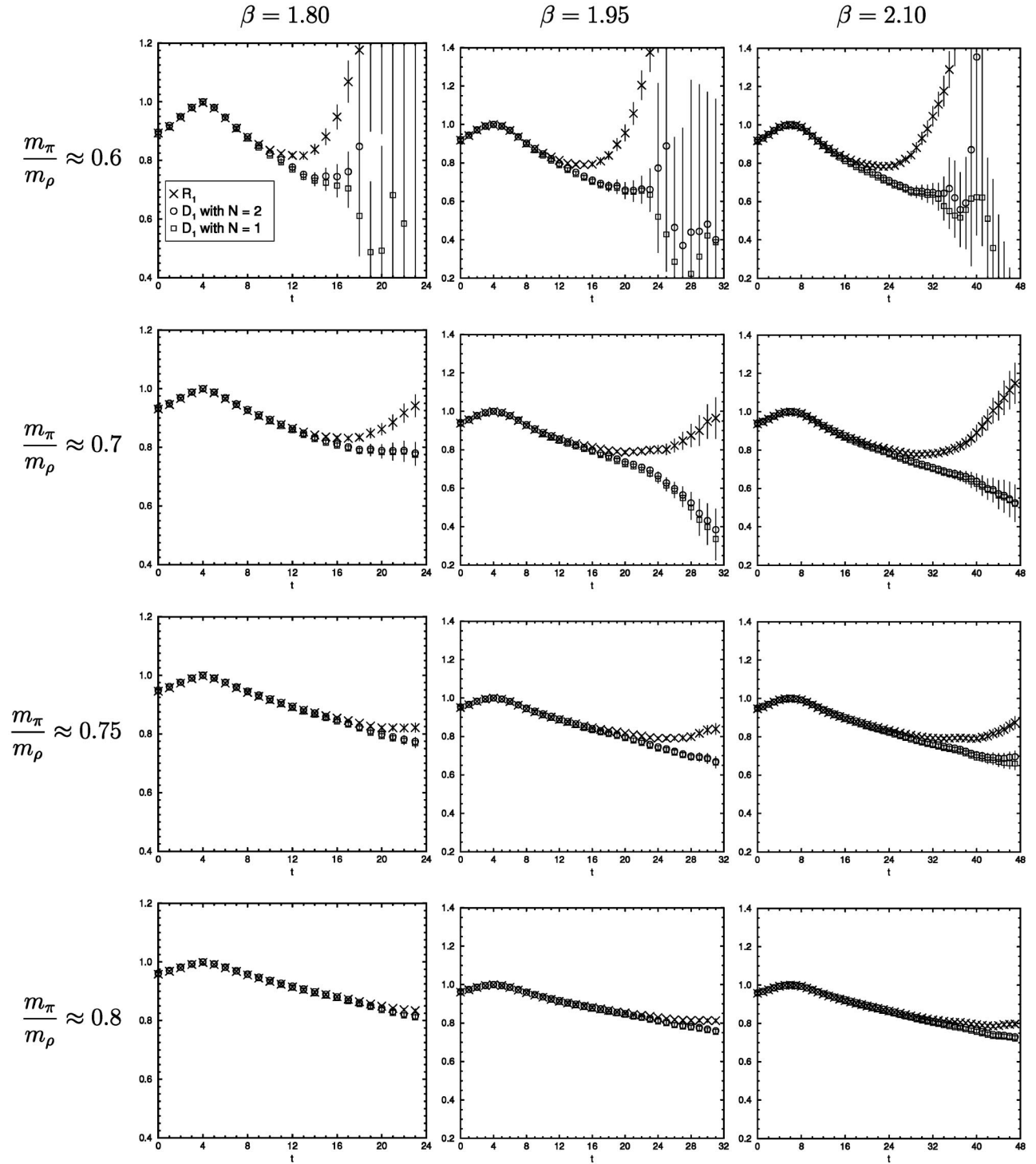
FIG. 4.    Ratio $R_n(t)$ and $D_n(t)$ for $n = 1$ in the center of mass system CM with energy state cut-off $N = 1, 2$. $m_\pi/m_\rho$ increases from top to bottom, while $\beta$ increases from left to right.

by comparing the results with $N = 1, 2$ and 3. The ratios $D_n(t)$ for $n = 0, 1$ for $m_\pi/m_\rho \approx 0.6$ at $\beta = 1.95$ are not clearly exponential in behavior. These results are not included in the following analysis considering that these defects are probably caused by insufficient statistics.

In order to show the effect of diagonalization in the L2 system clearly, we gather both ratios $R_n(t)$ and $D_n(t)$ for $n = 0$ and one in Fig. 9. The data at $\beta = 2.10$ for $m_\pi/m_\rho \approx 0.6$ is shown in the figure. Before the diagonalization the two ratios $R_n(t)$ have almost the same shape. After the diagonalization, however, the slope of
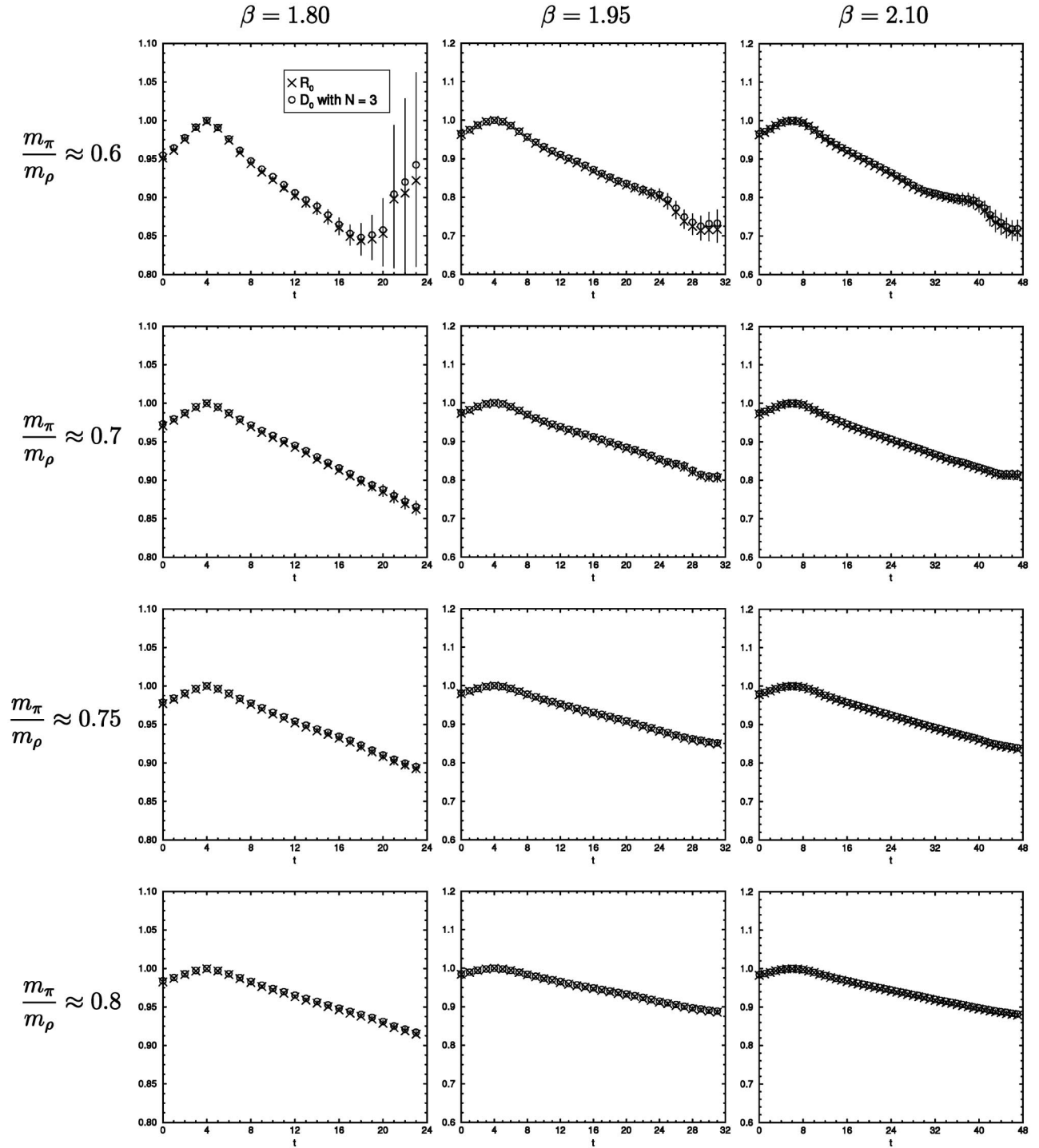
FIG. 5. Ratio $R_n(t)$ and $D_n(t)$ for $n = 0$ state in the laboratory system L1 with energy state cut-off $N = 3$. $m_\pi/m_\rho$ increases from top to bottom, while $\beta$ increases from left to right.

the ratios $D_n(t)$ for $n = 0$ decreases and that for $n = 1$ increases. This behavior can be understood by considering a simple eigenvalue problem for two degenerate states. We assume that the energies for $n = 0$ and one states in the L2 system have the same energy $E$ in the free two-pion case. Further we neglect the effects from higher energy states. This assumption is supported by the independence

on the cut-off $N$. In the interacting case the Hamiltonian $H$ for this system can be written as

$$H = \begin{pmatrix} E + \Delta & \beta \\ \beta & E + \Delta \end{pmatrix}, \qquad (29)$$

where the components of the Hamiltonian are defined by

FIG. 6. Ratio $R_n(t)$ and $D_n(t)$ for $n = 1$ state in the laboratory system L1 with energy state cut-off $N = 1$, 2 and 3. $m_\pi/m_\rho$ increases from top to bottom, while $\beta$ increases from left to right.

$H_{nm} \equiv \langle \Omega_n | H | \Omega_m \rangle$ with the noninteracting two-pion state $|\Omega_n\rangle$. The $\Delta$ and $\beta$ are unknown constants induced by the two-pion interaction. The constant $\Delta$ corresponds to the slopes of $R_n(t)$ up to $O[(\beta t)^2]$. The eigenvalues $\overline{E}$ of $H$ are given by

$$\overline{E} = E + \Delta \pm \beta. \tag{30}$$

The values of $\Delta \pm \beta$ correspond to the slopes of $D_n(t)$ for $n = 0$ and 1 in the figure. Here we can see that the existence of the off-diagonal component of the Hamiltonian $\beta$ causes a separation of $D_n(t)$.

Up to now we have shown that the ratios $D_n(t)$ for any $n$ in all the momentum systems behave as single exponential functions in $t$ and it is possible to extract the energy
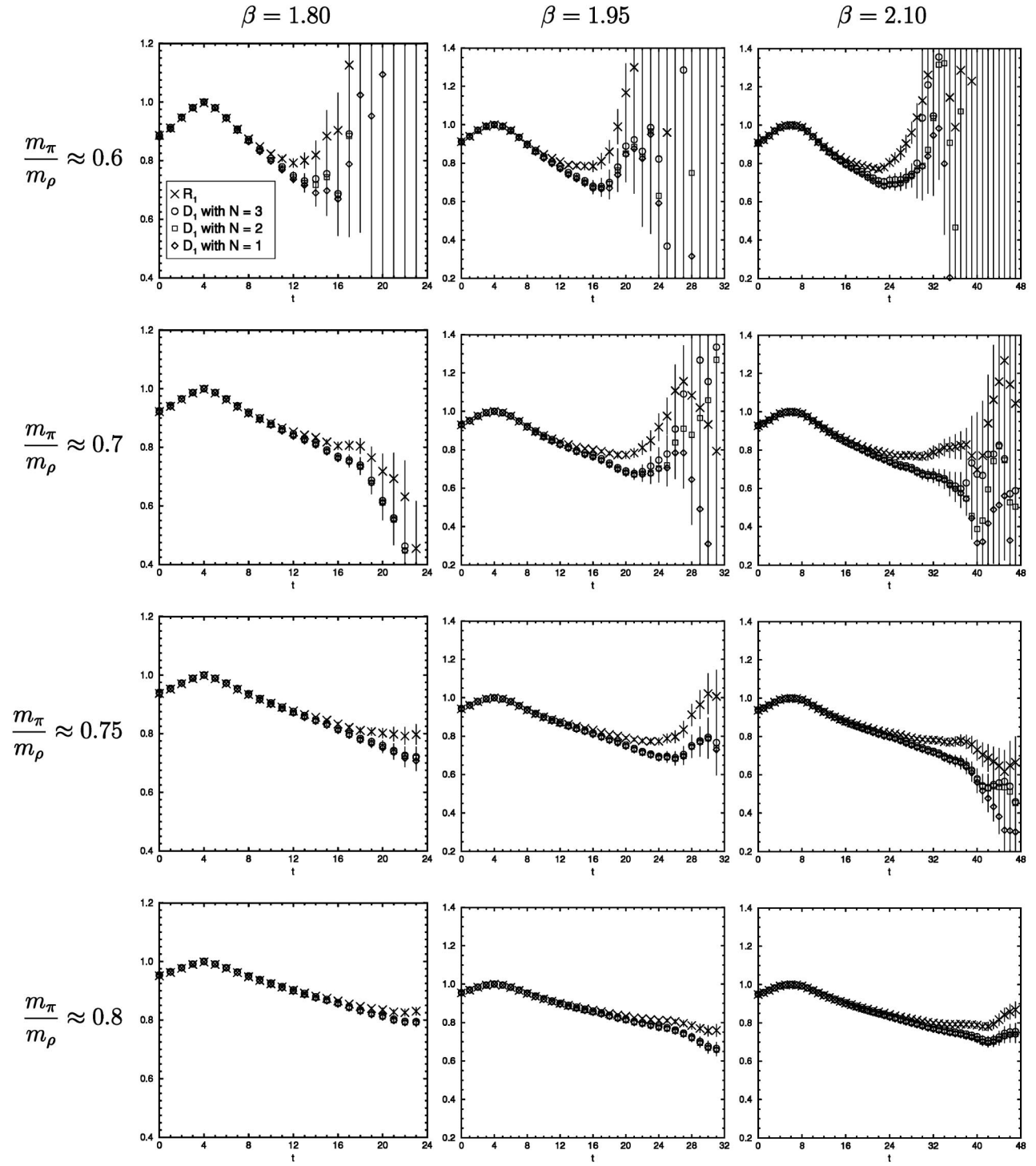
FIG. 7. Ratio $R_n(t)$ and $D_n(t)$ for $n = 0$ state in the laboratory system L2 with energy state cut off $N = 1, 2$ and $3$. $m_\pi/m_\rho$ increases from top to bottom, while $\beta$ increases from left to right.

shift $\Delta\overline{E}_n^{\mathbf{P}}$ by a single exponential fitting of the ratios. Our choice of the fitting range and the results of $\Delta\overline{E}_n^{\mathbf{P}}$ are summarized in Appendix B. The procedure of calculating the scattering phase shift $\delta(\overline{p}_n)$ from $\Delta\overline{E}_n^{\mathbf{P}}$ is the following. First, we construct the two-pion energy eigenvalue $\overline{E}_n^{\mathbf{P}}$ by $\overline{E}_n^{\mathbf{P}} = E_n^{\mathbf{P}} + \Delta\overline{E}_n^{\mathbf{P}}$, where $E_n^{\mathbf{P}}$ is the two-pion energy

in the free two-pion case. Then, we evaluate the Lorentz boost factor $\gamma$, the center of mass energy $\overline{E}_n$ and momentum $\overline{p}_n^2$ from $\overline{E}_n^{\mathbf{P}}$ by Eqs. (6)–(8). Finally, we obtain the phase shift $\delta(\overline{p}_n)$ by substituting $\overline{p}_n^2$ into the finite-volume formula given by Eqs. (3) and (9). The results are tabulated in Appendix B. In the Appendix we also quote the
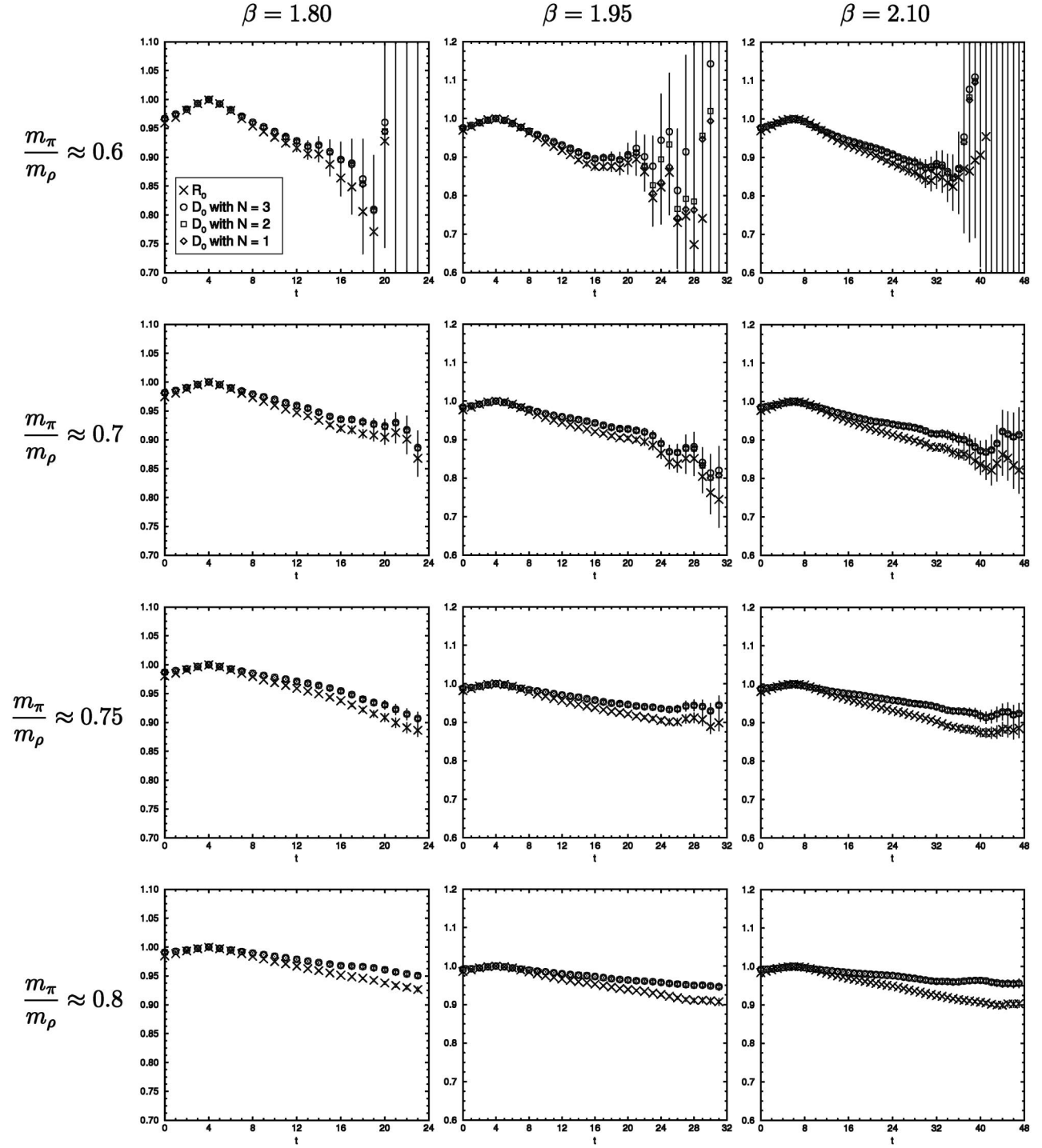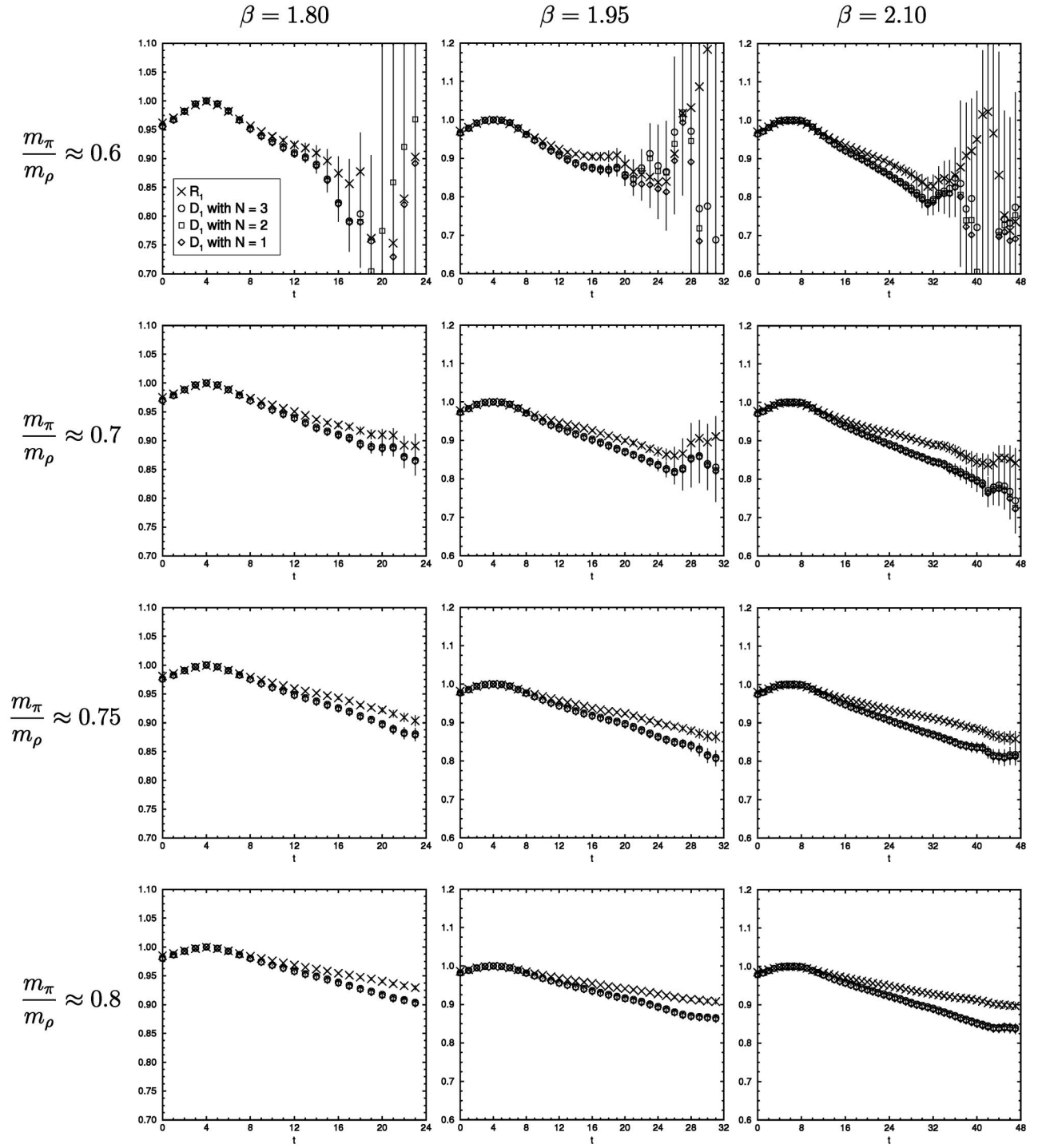
FIG. 8. Ratio $R_n(t)$ and $D_n(t)$ for $n = 1$ state in the laboratory system L2 with energy state cutoff $N = 1$, 2 and 3. $m_\pi/m_\rho$ increases from top to bottom, while $\beta$ increases from left to right.

scattering amplitude defined by

$$A(m_\pi, \overline{p}) = \frac{\tan\delta(\overline{p})}{\overline{p}} \cdot \frac{\overline{E}}{2}, \qquad (31)$$

where the amplitude is normalized as

$$\lim_{\overline{p} \to 0} A(m_\pi, \overline{p}) = a_0 m_\pi, \qquad (32)$$

with the scattering length $a_0$.

### B. Result for scattering length

In the CM system the momentum $\overline{p}^2$ for the ground state ($n = 0$) is very small as shown in Appendix B. Thus
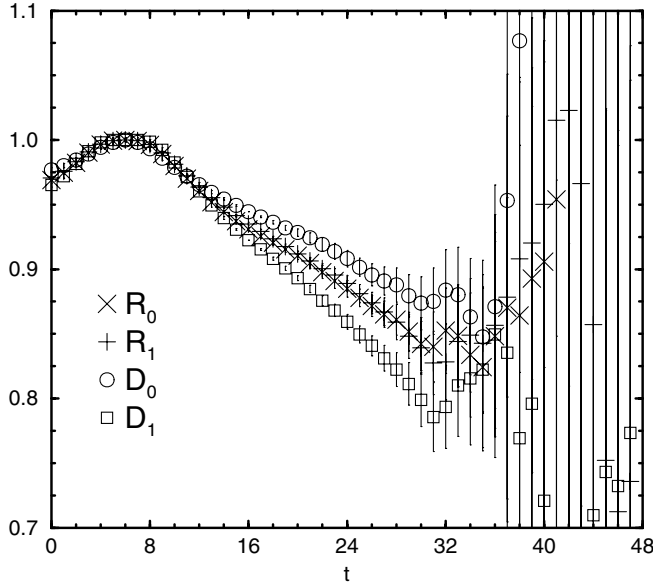
FIG. 9. Ratios $R_n(t)$ and $D_n(t)$ for $n = 0$ and 1 states in the laboratory system L2 with energy state cut-off $N = 3$ at $\beta = 2.10$ for $m_\pi/m_\rho \approx 0.6$.



FIG. 10. Results for $a_0/m_\pi$ at each $\beta$ and polynomial fits (dashed lines).

the scattering length $a_0$ can be evaluated from the scattering amplitude defined in Eq. (31) by $A(m_\pi, \overline{p}) \approx a_0 m_\pi$. In Fig. 10 we plot $a_0/m_\pi$ as a function of $m_\pi^2$ at each $\beta$, which are also tabulated in Appendix B denoted by $A(m_\pi, \overline{p})/m_\pi^2$. A significant curvature in the $m_\pi^2$ dependence at large $\beta$ is seen. This has not been clearly observed in the previous studies of the scattering length. The existence of a large curvature renders the chiral extrapolation of $a_0/m_\pi$ very difficult. In this work we attempt to fit the data with various fitting assumptions to obtain the scattering length at the physical pion mass $m_\pi = 0.14$ GeV.

The prediction of chiral perturbation theory (ChPT) for the $m_\pi^2$ dependence has been worked out by Gasser and Leutwyler [20]. In one-loop order it is given by

$$\frac{a_0}{m_\pi} = -\frac{1}{16\pi F^2}\left\{1 - \frac{m_\pi^2}{16\pi^2 F^2}\left[L(\mu) - C_L \cdot \log\frac{m_\pi^2}{\mu^2}\right]\right\},$$
(33)

where $F$ is the pseudoscalar decay constant in the chiral limit, $L(\mu)$ is a low energy constant at a scale $\mu$, and $C_L = 7/2$. It is clear that this one-loop formula cannot be naively applied to our results of the scattering length. As shown in Fig. 10 the dependence of $a_0/m_\pi$ on the lattice spacing is comparable to that of $m_\pi^2$. This implies that we should extrapolate our data with the formula including the $O(a)$ effect. Such a formula for the pseudoscalar mass and the decay constant has been obtained in a one-loop order of chiral perturbation theory for the Wilson type fermions [21], but for the scattering length is not yet available. Further, even if the $O(a)$ effect is negligible, it is not clear whether the formula of ChPT is applicable for our

data calculated in a heavy pion mass region, $m_\pi = 0.5 - 1.1$ GeV. Here, as a trial, we fit our data with the fitting assumption given by Eq. (33) with three unknown parameters $F$, $L(\mu)$ and $C_L$, and consider the dependence of fitted parameter values on the lattice spacing. The results are summarized in Table III, where the scale $\mu$ is fixed at $\mu = 1$ GeV in the analysis. We find a significant difference between $C_L$ obtained by the fitting and that of the prediction from ChPT ($C_L = 7/2$) at all $\beta$.

It is expected that the chiral breaking effect of the Wilson type fermion causes a divergence in the chiral limit as $a_0/m_\pi \propto 1/m_\pi^2$ [22]. The large curvature of the scattering length may originate from this effect. In Table IV we tabulate the results of the fitting with

$$\frac{a_0}{m_\pi} = \frac{A_{00}}{m_\pi^2} + A_{10} + A_{20}m_\pi^2.$$
(34)

The coefficient of the divergent term $A_{00}$, which comes from the chiral breaking effect, is expected to vanish in the continuum limit. However, our results for $A_{00}$ increases toward the continuum limit as opposed to the expectation. We consider that the effect of chiral breaking is not separated from the regular mass dependence. It is a very important future work to detect the divergence term through simulations with much higher statistics and closer to the chiral limit. We assume that the effect of chiral breaking is small in our simulation points in the following analysis.

Next we attempt to fit our data assuming the following polynomial function in $m_\pi^2$,

$$\frac{a_0}{m_\pi} = A_{10} + A_{20}m_\pi^2 + A_{30}m_\pi^4.$$
(35)

TABLE III.    Results of fitting for the scattering length $a_0/m_\pi$ obtained with the fitting function Eq. (33), where we set $\mu = 1$ GeV. The results at the physical pion mass are also tabulated.

| $\beta$ | $F$ GeV | $L(\mu)$ | $C_L$ | $\chi^2$/d.o.f. | $a_0/m_\pi[1/\text{GeV}^2]$ |
|---|---|---|---|---|---|
| 1.80 | 0.135(20) | 1.74(15) | 0.70(77) | 0.04 | $-1.04(40)$ |
| 1.95 | 0.1035(59) | 1.199(72) | 0.765(85) | 1.55 | $-1.76(20)$ |
| 2.10 | 0.0909(24) | 0.963(28) | 0.702(29) | 4.78 | $-2.26(11)$ |

TABLE IV.    Results of fitting for the scattering length $a_0/m_\pi$ obtained with a divergent form defined by Eq. (34).

| $\beta$ | $A_{00}$ | $A_{10}[1/\text{GeV}^2]$ | $A_{20}[1/\text{GeV}^4]$ | $\chi^2$/d.o.f. |
|---|---|---|---|---|
| 1.80 | $-0.033(89)$ | $-0.78(29)$ | 0.37(20) | 0.09 |
| 1.95 | $-0.184(57)$ | $-0.63(18)$ | 0.26(12) | 0.53 |
| 2.10 | $-0.273(35)$ | $-0.55(12)$ | 0.169(83) | 0.55 |

The results of the fitting are plotted in Fig. 10 and summarized in Table V. At $\beta = 2.10$ the value of $\chi^2$/d.o.f. is large. This indicates that the fitting including higher order terms, such as $m_\pi^6$ term or higher, is necessary to obtain a more precise value at the physical pion mass. Such fitting cannot be carried out in this work, because the number of our simulation points is only four.

In Refs. [2–4] the authors found that the mass dependence of the ratio $(f_\pi^{lat})^2 \cdot a_0/m_\pi$ was very small, where $f_\pi^{lat}$ is the decay constant measured on the lattice at each $m_\pi$. In Fig. 11 we plot the normalized scattering length defined by

$$\frac{\hat{a}_0}{m_\pi} = \left(\frac{f_\pi^{lat}}{f_\pi}\right)^2 \cdot \frac{a_0}{m_\pi}, \qquad (36)$$

where $f_\pi^{lat}$ is the decay constants measured in Ref. [16], which are tabulated in Table VI, and $f_\pi = 93$ MeV. The values of $\hat{a}_0/m_\pi$ are also tabulated in Appendix B; they are written under the column for $\hat{A}(m_\pi, \overline{p})/m_\pi^2$ defined by

$$\hat{A}(m_\pi, \overline{p}) = \left(\frac{f_\pi^{lat}}{f_\pi}\right)^2 \cdot A(m_\pi, \overline{p}). \qquad (37)$$

In the calculation of $\hat{a}_0/m_\pi$ the statistical errors of $f_\pi^{lat}$ are not included, since they are small compared with those of the scattering length. We observe in Fig. 11 that $\hat{a}_0/m_\pi$ is almost independent of $m_\pi^2$ within the statistical errors.



FIG. 11.    Results for $\hat{a}_0/m_\pi = (f_\pi^{lat}/f_\pi)^2 \cdot a_0/m_\pi$ with $f_\pi = 93$ MeV at each $\beta$ and constant fits (dashed lines).

This fact implies a strong correlation between the scattering length and the decay constant. The results of a constant fitting for $\hat{a}_0/m_\pi$ are also plotted in the figure and tabulated in Table VII. The values of $\chi^2$/d.o.f. are reasonably small. Especially at $\beta = 2.10$ it is much smaller than that of the polynomial fitting for $a_0/m_\pi$.

In Fig. 12 we present $a_0 m_\pi$ at the physical pion mass obtained by the polynomial fitting defined by Eq. (35) and $\hat{a}_0 m_\pi$ by the constant fitting as a function of the lattice spacing. We also plot the results of the continuum extrapolations, which are summarized in Table VIII. The prediction of ChPT [23]: $a_0 m_\pi = -0.0444(10)$ is denoted by the star symbol in the figure. We see large $O(a)$ effects in both $a_0 m_\pi$ and $\hat{a}_0 m_\pi$. Furthermore the $O(a)$ effect for

TABLE V.    Results of fitting for the scattering length $a_0/m_\pi$ obtained with a polynomial form defined by Eq. (35). The results at the physical pion mass are also tabulated.

| $\beta$ | $A_{10}[1/\text{GeV}^2]$ | $A_{20}[1/\text{GeV}^4]$ | $A_{30}[1/\text{GeV}^6]$ | $\chi^2$/d.o.f. | $a_0/m_\pi[1/\text{GeV}^2]$ |
|---|---|---|---|---|---|
| 1.80 | $-1.01(29)$ | 0.79(76) | $-0.20(46)$ | 0.02 | $-0.99(28)$ |
| 1.95 | $-1.57(14)$ | 1.58(33) | $-0.54(18)$ | 2.1 | $-1.54(13)$ |
| 2.10 | $-1.975(82)$ | 2.18(20) | $-0.82(11)$ | 8.2 | $-1.932(78)$ |

TABLE VI.  Pseudoscalar decay constant $f_\pi^{lat}$ measured on lattice [16]. Here $m_\pi^{phys}$ is the physical pion mass.

| | $\beta = 1.80$ | | $\beta = 1.95$ | | $\beta = 2.10$ |
|---|---|---|---|---|---|
| $m_\pi^2$ GeV$^2$ | $f_\pi^{lat}$ GeV | $m_\pi^2$ GeV$^2$ | $f_\pi^{lat}$ GeV | $m_\pi^2$ GeV$^2$ | $f_\pi^{lat}$ GeV |
| 1.128(1) | 0.2516(11) | 1.287(1) | 0.2190(16) | 1.332(2) | 0.1959(19) |
| 0.814(1) | 0.2279(14) | 0.857(1) | 0.1908(15) | 0.896(1) | 0.1739(21) |
| 0.571(1) | 0.1993(11) | 0.573(1) | 0.1650(14) | 0.605(2) | 0.1540(22) |
| 0.238(1) | 0.1613(15) | 0.291(2) | 0.1381(21) | 0.291(1) | 0.1214(19) |
| $(m_\pi^{phys})^2$ | 0.1287(33) | $(m_\pi^{phys})^2$ | 0.1054(47) | $(m_\pi^{phys})^2$ | 0.0895(45) |
| chiral limit | 0.1260(31) | chiral limit | 0.1032(47) | chiral limit | 0.0869(46) |

$\hat{a}_0 m_\pi$ is opposite to that of $a_0 m_\pi$ due to large $O(a)$ effects in $f_\pi^{lat}$. The difference between them decreases going toward the continuum limit.

As shown in Fig. 12 $\hat{a}_0 m_\pi$ in the continuum limit is closer to the prediction of ChPT than that of $a_0 m_\pi$. We should note, however, that the decay constant is introduced in $\hat{a}_0 / m_\pi$ to compensate the mass dependence of the scattering length. Extrapolations only with the scattering length are difficult as discussed before.

The decay constant measured in the previous work of Ref. [16], is tabulated in Table VI. As shown in the table,

TABLE VII.  Results of a constant fit for $\hat{a}_0 = (f_\pi^{lat}/f_\pi)^2 \cdot a_0/m_\pi$.

| $\beta$ | $\hat{a}_0/m_\pi[1/\text{GeV}^2]$ | $\chi^2/$d.o.f. |
|---|---|---|
| 1.80 | $-2.83(13)$ | 0.27 |
| 1.95 | $-2.543(73)$ | 0.92 |
| 2.10 | $-2.449(40)$ | 0.54 |

the value in the continuum limit seems not consistent with the experiment $f_\pi = 93$ MeV. One of possible reasons for this discrepancy is an uncertainty of the renormalization factor for the axial vector current; in Ref. [16] the perturbative renormalization factor was used. This causes a large uncertainty in the prediction of the scattering length in the continuum limit. In order to obtain more reliable predictions for the physical scattering length, a nonperturbative determination of the renormalization factor and higher statics calculations of the scattering length closer to the physical pion mass and the continuum limit are needed. Here we present the two values estimated by $a_0 m_\pi$ and $\hat{a}_0 m_\pi = (f_\pi^{lat}/f_\pi)^2 \cdot a_0 m_\pi$ as our results for the scattering length in this work with the provisions noted above:

$$a_0 m_\pi = -0.0558(56), \tag{38}$$

$$\hat{a}_0 m_\pi = -0.0413(29). \tag{39}$$

### C. Result for scattering phase shift

The results for the scattering amplitudes $A(m_\pi, \overline{p})$ defined by Eq. (31) are plotted in Fig. 13. The $CM_n$ in the top left figure refers to the amplitude obtained from the $n$th energy eigenstate state in the CM system, and the $L1_n$ and $L2_n$ to those in each laboratory system. The ordering of the amplitude, $CM_0$, $L1_0$, $L2_0$, $\cdots$, $L1_1$, in the other figures is the same. The open symbols are excluded from the following analysis. They correspond to the data in which we cannot clearly observe a single exponential time be-
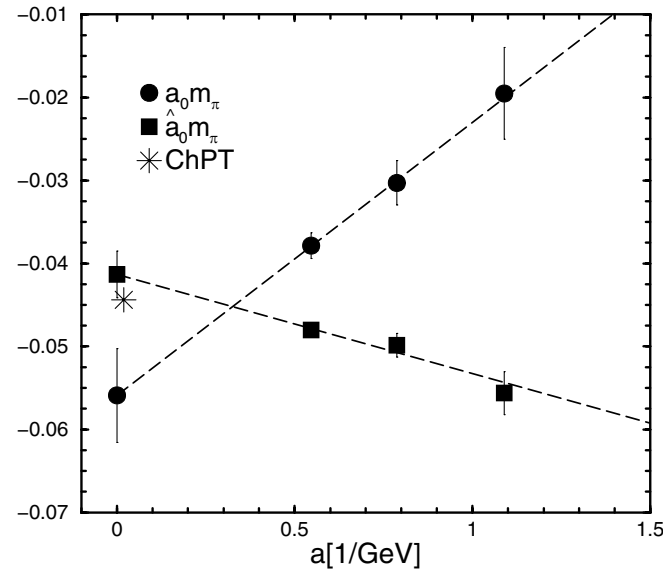


FIG. 12.  Results for $a_0 m_\pi$ and $\hat{a}_0 m_\pi = (f_\pi^{lat}/f_\pi)^2 \cdot a_0/m_\pi$ at the physical pion mass as functions of lattice spacing.

TABLE VIII.  Results of the continuum extrapolations for the two scattering lengths $a_0 m_\pi$ and $\hat{a}_0 m_\pi = (f_\pi^{lat}/f_\pi)^2 \cdot a_0 m_\pi$ as a function $A + aB$. Here $A$ corresponds to the scattering length in the continuum limit.

| | $A$ | $B$ GeV | $\chi^2/$d.o.f. |
|---|---|---|---|
| $a_0 m_\pi$ | $-0.0558(56)$ | 0.0328(86) | 0.02 |
| $\hat{a}_0 m_\pi$ | $-0.0413(28)$ | $-0.0119(43)$ | 0.65 |
| ChPT | $-0.0444(10)$ | | |
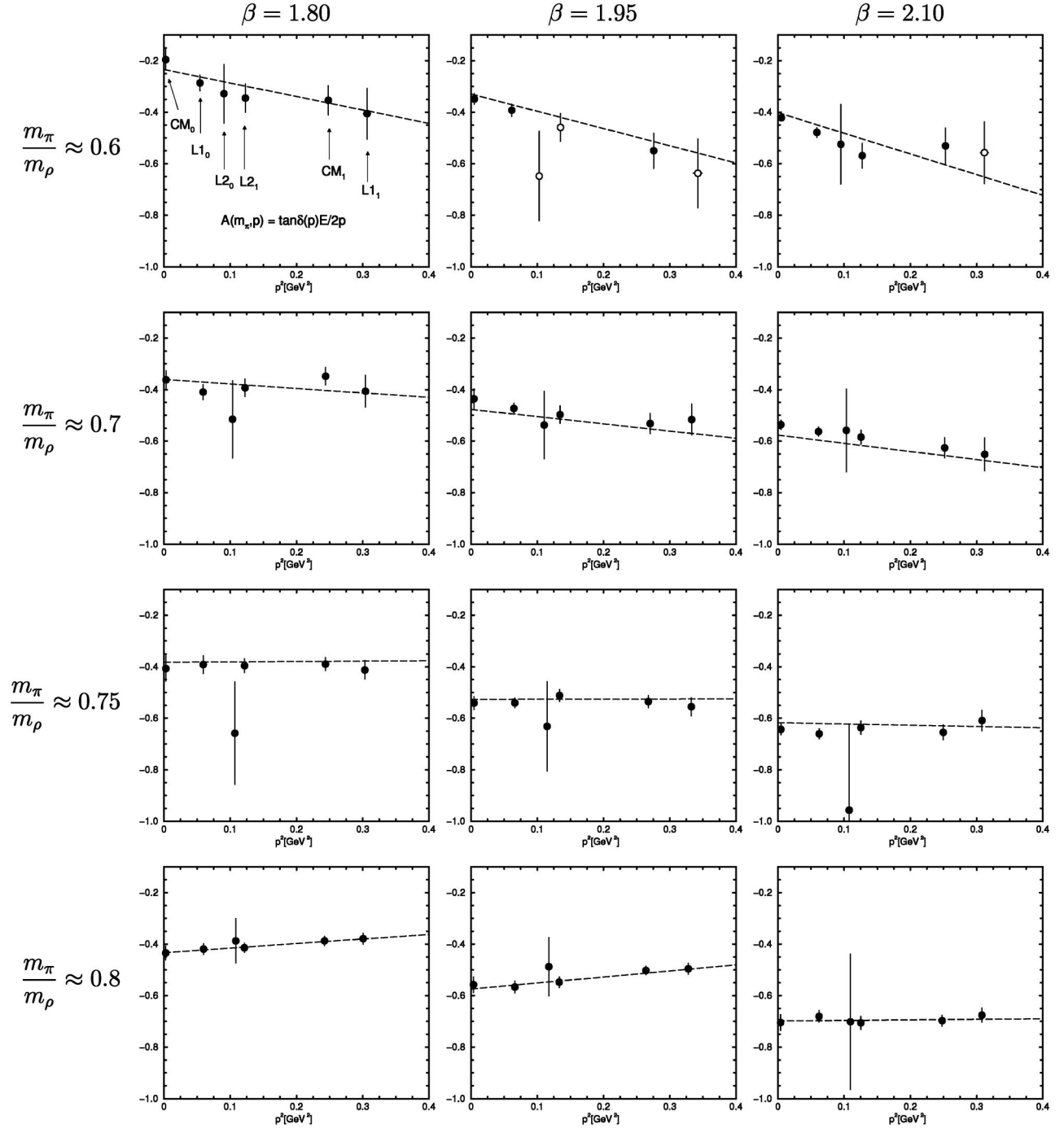
FIG. 13.   Scattering amplitude $A(m_\pi, \overline{p}) = \tan\delta(\overline{p})/\overline{p} \cdot \overline{E}/2$. $CM_n$ refers to the amplitude obtained from the $n$th state in the center of mass system, and $L1_n$ and $L2_n$ to those in the laboratory systems. Open symbols are excluded from the global fit. $m_\pi/m_\rho$ increases from top to bottom, while $\beta$ increases from left to right.

havior of $D_n(t)$ as noted in Sec. IVA. The values of $A(m_\pi, \overline{p})$ are tabulated in Appendix B.

We obtain the scattering phase shift $\delta(\overline{p})$ at the physical pion mass for various momenta $\overline{p}$ in the continuum limit by the following procedure. First we fit the results of $A(m_\pi, \overline{p})$ with the following fitting assumption at each lattice spacing,

$$A(m_\pi, \overline{p}) = A_{10}m_\pi^2 + A_{20}m_\pi^4 + A_{30}m_\pi^6 + A_{01}\overline{p}^2 + A_{11}m_\pi^2\overline{p}^2 + A_{21}m_\pi^4\overline{p}^2. \tag{40}$$

Then we evaluate the amplitudes at the physical pion mass for various momenta at each lattice spacing from the constants $A_{ij}$ obtained by the fitting. Finally the

TABLE IX. Results of a polynomial fit of $m_\pi^2$ and $\overline{p}^2$ for the scattering amplitude defined by $A(m_\pi, \overline{p}) = \tan\delta(\overline{p})/\overline{p} \cdot \overline{E}/2$.

| $\beta$ | 1.80 | 1.95 | 2.10 |
|---|---|---|---|
| $A_{10}[1/\text{GeV}^2]$ | $-1.33(21)$ | $-1.52(12)$ | $-1.899(84)$ |
| $A_{20}[1/\text{GeV}^4]$ | $1.62(53)$ | $1.51(29)$ | $2.00(20)$ |
| $A_{30}[1/\text{GeV}^6]$ | $-0.69(31)$ | $-0.52(16)$ | $-0.73(11)$ |
| $A_{01}[1/\text{GeV}^2]$ | $-0.83(44)$ | $-1.18(47)$ | $-1.43(40)$ |
| $A_{11}[1/\text{GeV}^4]$ | $1.4(12)$ | $1.9(11)$ | $2.48(95)$ |
| $A_{21}[1/\text{GeV}^6]$ | $-0.46(83)$ | $-0.65(61)$ | $-1.04(52)$ |
| $\chi^2/\text{d.o.f.}$ | $0.90$ | $0.64$ | $1.33$ |

continuum extrapolation is taken for these amplitudes at each momentum. The results of the fitting with the assumption Eq. (40) are plotted in Fig. 13, and the constants $A_{ij}$ are tabulated together with $\chi^2/\text{d.o.f.}$ in Table IX. The values of $\chi^2/\text{d.o.f.}$ are reasonably small at all $\beta$ in contrast to the polynomial fit for the scattering length where $\chi^2/\text{d.o.f.}$ at $\beta = 2.10$ is large as shown in Sec. IV B.

It is possible to make a global polynomial fit with the assumption Eq. (40) for all momentum systems, so that we do not need to introduce the decay constant measured on the lattice as for the scattering length in the previous section. For consistency of the analysis, we also analyze $\hat{A}(m_\pi, \overline{p})$ defined by Eq. (37). Here we assume the same fitting assumption Eq. (40), but set $A_{20} = A_{30} = A_{21} = 0$, since the mass dependence becomes mild by a compensation with that of the decay constant also in this case. The fit results are tabulated in Table X.

In Fig. 14 both amplitudes at the physical pion mass for various momenta are plotted as a function of the lattice spacing, together with the continuum extrapolations. Here we choose three momenta, $\overline{p}^2 = 0$, 0.06 and 0.26 GeV$^2$ which are roughly equal to the momenta of CM$_0$, L1$_0$ and CM$_1$, respectively. The result at $\overline{p}^2 = 0$ gives the scattering length $a_0 m_\pi$. We also plot the scattering lengths obtained in the previous section, which are calculated from the data only in CM$_0$. As shown in the figure they are consistent within the statistical error at each lattice spacing. There are slight differences, however, in the continuum limit between the results obtained from all momentum system at $\overline{p}^2 = 0$ given by

$$a_0 m_\pi = -0.0484(49), \qquad (41)$$

TABLE X. Results of a polynomial fit of $m_\pi^2$ and $\overline{p}^2$ for the normalized scattering amplitude defined by $\hat{A}(m_\pi, \overline{p}) = (f_\pi^{lat}/f_\pi)^2 \cdot \tan\delta(\overline{p})/\overline{p} \cdot \overline{E}/2$.

| $\beta$ | 1.80 | 1.95 | 2.10 |
|---|---|---|---|
| $\hat{A}_{10}[1/\text{GeV}^2]$ | $-2.84(10)$ | $-2.546(59)$ | $-2.438(38)$ |
| $\hat{A}_{01}[1/\text{GeV}^2]$ | $-2.78(59)$ | $-2.84(44)$ | $-2.14(37)$ |
| $\hat{A}_{11}[1/\text{GeV}^4]$ | $3.67(76)$ | $3.36(49)$ | $2.05(43)$ |
| $\chi^2/\text{d.o.f.}$ | $0.77$ | $0.50$ | $0.75$ |
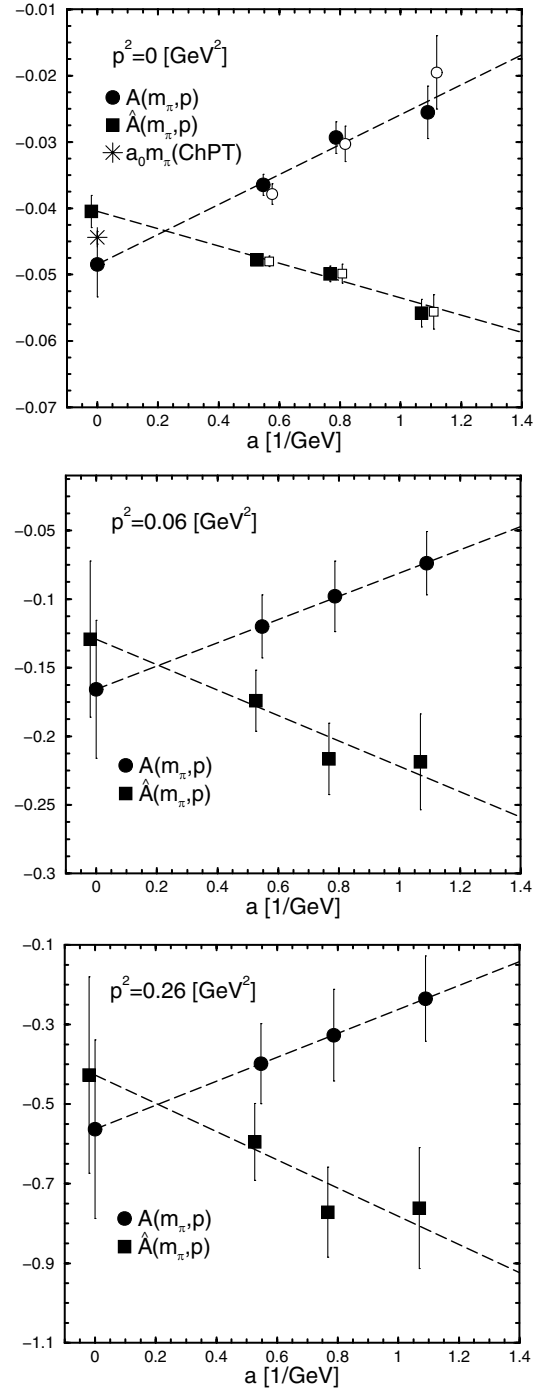


FIG. 14. Scattering amplitudes $A(m_\pi, \overline{p}) = \tan\delta(\overline{p})/\overline{p} \cdot \overline{E}/2$ and $\hat{A}(m_\pi, \overline{p}) = (f_\pi^{lat}/f_\pi)^2 \cdot A(m_\pi, \overline{p})$ at the physical pion mass and several momenta. The pseudoscalar decay constant $f_\pi^{lat}$ is measured on lattice and $f_\pi = 93$ MeV. Open symbols are $a_0 m_\pi$ and $\hat{a}_0 m_\pi$ taken from Fig. 12.

$$\hat{a}_0 m_\pi = -0.0404(24), \qquad (42)$$

and the results from only the CM$_0$ data given by Eqs. (38) and (39). We consider that these discrepancies represent the uncertainty of the continuum extrapolations using

data at only three lattice spacings, e.g., the number of degrees of freedom for the extrapolation is one, far from the continuum limit. The difference of the two amplitudes tends to vanish in the continuum limit. As mentioned in the previous section; however, there is an uncertainty in the determination of the decay constant on the lattice. Thus we do not use $\hat{A}(m_\pi, \overline{p})$ to obtain the final results of the phase shift.

In Fig. 15 the result of the phase shift obtained from the scattering amplitude $A(m_\pi, \overline{p})$ in the continuum limit is presented by a dashed line, and associated by a band of error bars. The values of the phase shift at several momenta are tabulated in Table XI. Our results are compared with the solid curve [23] estimated with the experimental input, and the experimental results [24,25]. The result in the continuum limit agrees with experiment, although the errors of our result are large. In order to obtain more precise results simulations are needed closer to the chiral and the continuum limits with much higher statistics.

## V. CONCLUSIONS

In this article we have presented our results for the $I = 2$ $S$-wave $\pi\pi$ scattering phase shift in the continuum limit calculated with two-flavor dynamical quark effects. While errors are not small, it is very encouraging to find that the phase shift in the continuum limit shows a reasonable agreement with experiment.

The large errors of our final results arise from the chiral extrapolation and the continuum extrapolation. In

TABLE XI. Scattering phase shift $\delta(\overline{p})$ in the continuum limit at the physical pion mass.

| $\overline{p}^2$ GeV$^2$ | $\sqrt{s}$ GeV | $\delta(\overline{p})$ [degrees] |
|---|---|---|
| 0.020 | 0.40 | $-3.50(64)$ |
| 0.072 | 0.60 | $-9.5(30)$ |
| 0.140 | 0.80 | $-16.9(64)$ |
| 0.232 | 1.00 | $-25(10)$ |

order to obtain more precise results, simulations are needed closer to the chiral and the continuum limits with much higher statistics. Technically, investigating the correlation we found between the scattering length and the decay constant measured on lattice, and detecting effects of chiral symmetry breaking with Wilson fermion action are important open issues for future work.

In addition to being a first calculation of realistic scattering quantity based on first principles of QCD, the importance of the present work resides in actually showing that various technical methods, such as diagonalization of pion four-point functions and use of laboratory systems, necessary for practical success of the finite-volume methods work. Thus we can envisage a perspective toward extension of the present work for calculations of other important scattering process, such as $I = 1$ and $I = 0$ two-pion systems, systems including unstable particles, and scattering with baryons, which are richer in physics content. These processes are more difficult from the point of calculations, however, and algorithmic advances are probably needed to evaluate complicated diagrams.
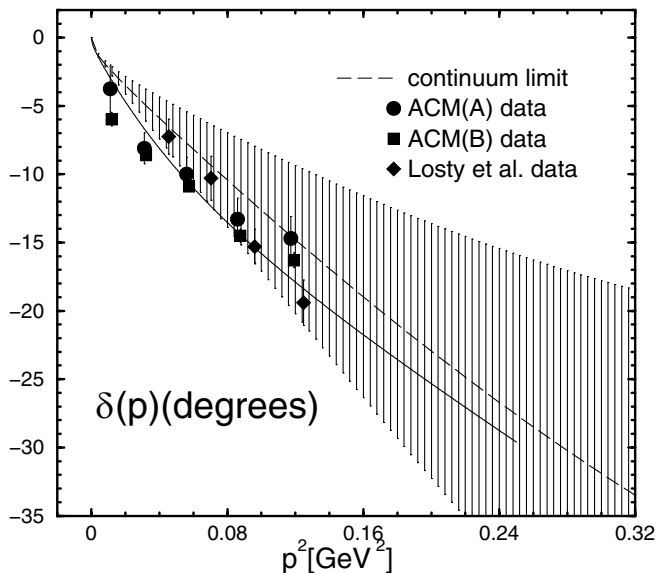
## ACKNOWLEDGMENTS

FIG. 15. Results of the scattering phase shifts in the continuum limit (dashed line) and a band of error bars. Solid line [23] is estimated with experimental inputs using the Roy equation. Symbols represent data of Aachen-Cern-Munich Collaboration [24] and of Losty *et al.* [25].

## APPENDIX A: CALCULATION METHOD OF ZETA FUNCTION

In this Appendix we introduce methods for the numerical evaluation of the zeta function $Z_{00}^{\mathbf{d}}(s; \overline{m})$ defined in Eq. (10). This problem has already been discussed by Lüscher in Appendix A of Ref. [10] and in Appendix C of Ref. [11] for the center of mass system, and by Rummukainen and Gottlieb in Sec. 5.2 of Ref. [17] for general systems. Our basic idea is the same, but our final expression for the zeta function is simpler and more efficient for numerical evaluations. (We find that there are some typographical errors in the expression of the zeta function in Ref. [17]). Very recently Li and Liu have

reported a similar calculation method of the zeta function in asymmetric box [26].

The definition of the zeta function $Z_{00}^{\mathbf{d}}(s;\overline{m})$ is

$$\sqrt{4\pi} \cdot Z_{00}^{\mathbf{d}}(s;\overline{m}) = \sum_{\mathbf{r}\in P^{\mathbf{d}}} (r^2 - \overline{m})^{-s}. \qquad (A1)$$

The summation for $\mathbf{r}$ is carried out over the set

$$P^{\mathbf{d}} = \{\mathbf{r}|\mathbf{r} = \hat{\gamma}^{-1}(\mathbf{n} + \mathbf{d}/2), \mathbf{n} \in Z^3\}. \qquad (A2)$$

The operation $\hat{\gamma}^{-1}$ is the inverse Lorentz transformation: $\hat{\gamma}^{-1}\mathbf{n} = 1/\gamma \cdot \mathbf{n}_{\parallel} + \mathbf{n}_{\perp}$ where $\mathbf{n}_{\parallel} = (\mathbf{n}\cdot\mathbf{d})\mathbf{d}/d^2$ is the parallel component and $\mathbf{n}_{\perp} = \mathbf{n} - \mathbf{n}_{\parallel}$ the perpendicular component of $\mathbf{n}$ in the direction $\mathbf{d}$. The zeta function $Z_{00}^{\mathbf{d}}(s;\overline{m})$ takes a finite value for $\mathrm{R}es > 3/2$, and

$Z_{00}^{\mathbf{d}}(1;\overline{m})$, which is used to obtain the scattering phase shift in Eq. (9), is defined by the analytic continuation from the region $\mathrm{R}es > 3/2$.

First we divide the summation in $Z_{00}^{\mathbf{d}}(s;\overline{m})$ into two parts as

$$\sum_{\mathbf{r}}(r^2 - \overline{m})^{-s} = \sum_{r^2 < \overline{m}}(r^2 - \overline{m})^{-s} + \sum_{r^2 > \overline{m}}(r^2 - \overline{m})^{-s}, \qquad (A3)$$

where the summation over $\mathbf{r}$ is carried out with $\mathbf{r} \in P^{\mathbf{d}}$. The second term can be written in an integral form as follows,

$$\sum_{r^2 > \overline{m}}(r^2 - \overline{m})^{-s} = \frac{1}{\Gamma(s)}\sum_{r^2 > \overline{m}}\int_0^\infty \mathrm{d}t\, t^{s-1}e^{-t(r^2-\overline{m})} = \frac{1}{\Gamma(s)}\sum_{r^2 > \overline{m}}\left[\int_0^1 \mathrm{d}t\, t^{s-1}e^{-t(r^2-\overline{m})} + \int_1^\infty \mathrm{d}t\, t^{s-1}e^{-t(r^2-\overline{m})}\right]$$

$$= \frac{1}{\Gamma(s)}\int_0^1 \mathrm{d}t\, t^{s-1}e^{t\overline{m}}\sum_{\mathbf{r}}e^{-tr^2} - \sum_{r^2 < \overline{m}}(r^2 - \overline{m})^{-s} + \sum_{j=1}^s \frac{1}{(s-j)!}. \qquad (A4)$$

The second term cancels out the first term in Eq. (A3). Next we rewrite the first term in Eq. (A4) by the Poisson's summation formula

$$\sum_{\mathbf{n}\in Z^3} f(\mathbf{n}) = \sum_{\mathbf{n}\in Z^3}\int \mathrm{d}^3 x f(\mathbf{x})e^{i2\pi\mathbf{n}\cdot\mathbf{x}}, \qquad (A5)$$

and integrating over $\mathbf{x}$ yields,

$$\frac{1}{\Gamma(s)}\int_0^1 \mathrm{d}t\, t^{s-1}e^{t\overline{m}}\sum_{\mathbf{r}}e^{-tr^2} = \frac{\gamma}{\Gamma(s)}\int_0^1 \mathrm{d}t\, t^{s-1}e^{t\overline{m}}\left(\frac{\pi}{t}\right)^{3/2}\sum_{\mathbf{n}\in Z^3}(-1)^{\mathbf{n}\cdot\mathbf{d}}e^{-\pi^2(\hat{\gamma}\mathbf{n})^2/t}. \qquad (A6)$$

The divergence at $s = 1$ comes from the $\mathbf{n} = \mathbf{0}$ part of the integrand on the right-hand side. We divide the integrand into a divergent part ($\mathbf{n} = \mathbf{0}$) and a finite part ($\mathbf{n} \neq \mathbf{0}$). The divergent part can be evaluated for $\mathrm{R}es > 3/2$ as

$$\int_0^1 \mathrm{d}t\, t^{s-1}e^{t\overline{m}}\left(\frac{\pi}{t}\right)^{3/2} = \sum_{l=0}^\infty \frac{\pi^{3/2}}{s+l-3/2}\frac{\overline{m}^l}{l!}. \qquad (A7)$$

The right had side of this equation takes a finite value at $s = 1$.

Finally by gathering all terms we obtain the following expression for the zeta function at $s = 1$,

$$\sqrt{4\pi} \cdot Z_{00}^{\mathbf{d}}(1;\overline{m}) = \sum_{\mathbf{r}}\frac{e^{-(r^2-\overline{m})}}{r^2 - \overline{m}} + \gamma\int_0^1 \mathrm{d}t\, e^{t\overline{m}}\left(\frac{\pi}{t}\right)^{3/2}\sum_{\mathbf{n}\in Z^3}{}'(-1)^{\mathbf{n}\cdot\mathbf{d}}e^{-\pi^2(\hat{\gamma}\mathbf{n})^2/t} + \gamma\sum_{l=0}^\infty \frac{\pi^{3/2}}{l-1/2}\frac{\overline{m}^l}{l!}, \qquad (A8)$$

where $\sum_{\mathbf{n}\in Z^3}'$ is the summation without $\mathbf{n} = \mathbf{0}$.

Substituting $\mathbf{d} = 0$ and $\gamma = 1$ into the above expression, we obtain the representation of the zeta function in the center of mass system appeared in Eq. (3)

$$\sqrt{4\pi} \cdot Z_{00}(1;\overline{m}) = \sum_{\mathbf{n}\in Z^3}{}'\frac{e^{-(n^2-\overline{m})}}{n^2 - \overline{m}} + \int_0^1 \mathrm{d}t\, e^{t\overline{m}}\left(\frac{\pi}{t}\right)^{3/2}\sum_{\mathbf{n}}{}'e^{-\pi^2 n^2/t} + \sum_{l=0}^\infty \frac{\pi^{3/2}}{l-1/2}\frac{\overline{m}^l}{l!}. \qquad (A9)$$

## APPENDIX B. TABLE FOR RESULTS OF SCATTERING LENGTH AND SCATTERING PHASE SHIFT IN EACH SYSTEM

In Tables XII, XIII, XIV, XV, XVI, and XVII we tabulate fitting ranges, energy shift $\Delta\overline{E}_n^{\mathbf{P}}$, center of mass

momentum $\overline{p}^2$, Lorentz boost factor $\gamma$, scattering phase shift $\delta(\overline{p})$, scattering amplitude $A(m_\pi, \overline{p})$ defined by Eq. (31), and normalized scattering amplitude $\hat{A}(m_\pi, \overline{p})$ defined by Eq. (37) in each system for the ground $n = 0$ and first excited $n = 1$ states.

TABLE XII.    Results for $n = 0$ state in the center of mass system CM with energy state cut-off $N = 2$. Two scattering amplitudes are defined by $A(m_\pi, \overline{p}_n) = \tan\delta(\overline{p}_n)/\overline{p}_n \cdot \overline{E}_n/2$ and $\hat{A}(m_\pi, \overline{p}_n) = (f_\pi^{lat}/f_\pi)^2 \cdot A(m_\pi, \overline{p}_n)$, where $f_\pi^{lat}$ is the pseudoscalar decay constant measured on lattice and $f_\pi = 93$ MeV.

| $\beta = 1.80$ | $\kappa$ | 0.1464 | 0.1445 | 0.1430 | 0.1409 |
|---|---|---|---|---|---|
| $a^{-1} = 0.9176(93)$ GeV | $m_\pi/m_\rho$ | 0.547(4) | 0.694(2) | 0.753(1) | 0.807(1) |
| | $m_\pi^2$ GeV$^2$ | 0.238(1) | 0.571(1) | 0.814(1) | 1.128(1) |
| Fitting Range | | 10–20 | 12–20 | 12–20 | 12–20 |
| $\Delta\overline{E}_n^{\mathbf{P}}$ | [$\times 10^{-3}$ GeV] | 4.61(98) | 3.62(39) | 2.84(37) | 2.17(14) |
| $\overline{p}_n^2$ | [$\times 10^{-4}$ GeV2] | 24.5(52) | 29.9(32) | 27.9(37) | 25.1(17) |
| $\delta(\overline{p}_n)$ | [degrees] | −1.13(34) | −1.49(22) | −1.36(25) | −1.17(11) |
| $A(m_\pi, \overline{p}_n)$ | | −0.196(38) | −0.362(35) | −0.406(49) | −0.434(26) |
| $\hat{A}(m_\pi, \overline{p}_n)$ | | −0.59(11) | −1.66(16) | −2.44(29) | −3.17(19) |
| $A(m_\pi, \overline{p}_n)/m_\pi^2$ | [1/GeV$^2$] | −0.82(16) | −0.633(62) | −0.499(60) | −0.384(23) |
| $\hat{A}(m_\pi, \overline{p}_n)/m_\pi^2$ | [1/GeV$^2$] | −2.47(48) | −2.91(28) | −3.02(33) | −2.83(17) |
| $\beta = 1.95$ | $\kappa$ | 0.1410 | 0.1400 | 0.1390 | 0.1375 |
| $a^{-1} = 1.268(13)$ GeV | $m_\pi/m_\rho$ | 0.582(3) | 0.690(1) | 0.752(1) | 0.804(1) |
| | $m_\pi^2$ GeV$^2$ | 0.291(2) | 0.573(1) | 0.857(1) | 1.287(1) |
| Fitting Range | | 12–23 | 13–25 | 13–25 | 13–25 |
| $\Delta\overline{E}_n^{\mathbf{P}}$ | [$\times 10^{-3}$ GeV] | 10.95(73) | 6.89(69) | 5.74(30) | 3.86(23) |
| $\overline{p}_n^2$ | [$\times 10^{-4}$ GeV$^2$] | 46.7(31) | 41.2(41) | 41.9(22) | 34.5(21) |
| $\delta(\overline{p}_n)$ | [degrees] | −2.50(23) | −2.10(29) | −2.16(15) | −1.65(14) |
| $A(m_\pi, \overline{p}_n)$ | | −0.348(20) | −0.436(38) | −0.540(25) | −0.557(30) |
| $\hat{A}(m_\pi, \overline{p}_n)$ | | −0.769(45) | −1.37(12) | −2.27(10) | −3.09(17) |
| $A(m_\pi, \overline{p}_n)/m_\pi^2$ | [1/GeV$^2$] | −1.195(70) | −0.759(67) | −0.630(29) | −0.433(23) |
| $\hat{A}(m_\pi, \overline{p}_n)/m_\pi^2$ | [1/GeV$^2$] | −2.63(15) | −2.39(21) | −2.65(12) | −2.40(13) |
| $\beta = 2.10$ | $\kappa$ | 0.1382 | 0.1374 | 0.1367 | 0.1357 |
| $a^{-1} = 1.833(22)$ GeV | $m_\pi/m_\rho$ | 0.576(3) | 0.691(3) | 0.755(2) | 0.806(1) |
| | $m_\pi^2$ GeV$^2$ | 0.291(1) | 0.605(2) | 0.896(1) | 1.332(2) |
| Fitting Range | | 18–35 | 18–35 | 18–35 | 18–35 |
| $\Delta\overline{E}_n^{\mathbf{P}}$ | [$\times 10^{-3}$ GeV] | 17.33(54) | 10.48(42) | 8.49(32) | 6.16(30) |
| $\overline{p}_n^2$ | [$\times 10^{-4}$ GeV$^2$] | 51.3(16) | 44.6(17) | 44.0(16) | 38.9(19) |
| $\delta(\overline{p}_n)$ | [degrees] | −3.17(13) | −2.62(14) | −2.57(13) | −2.17(14) |
| $A(m_\pi, \overline{p}_n)$ | | −0.421(12) | −0.536(18) | −0.643(20) | −7.04(30) |
| $\hat{A}(m_\pi, \overline{p}_n)$ | | −0.718(20) | −1.471(49) | −2.251(72) | −3.12(13) |
| $A(m_\pi, \overline{p}_n)/m_\pi^2$ | [1/GeV$^2$] | −1.444(38) | −0.885(31) | −0.718(23) | −0.528(23) |
| $\hat{A}(m_\pi, \overline{p}_n)/m_\pi^2$ | [1/GeV$^2$] | −2.462(66) | −2.429(85) | −2.512(82) | −2.34(10) |

TABLE XIII. Results for $n = 1$ state in the center of mass system CM with energy state cut-off $N = 2$. Two scattering amplitudes are defined by $A(m_\pi, \overline{p}_n) = \tan\delta(\overline{p}_n)/\overline{p}_n \cdot \overline{E}_n/2$ and $\hat{A}(m_\pi, \overline{p}_n) = (f_\pi^{lat}/f_\pi)^2 \cdot A(m_\pi, \overline{p}_n)$, where $f_\pi^{lat}$ is the pseudoscalar decay constant measured on lattice and $f_\pi = 93$ MeV.

| $\beta = 1.80$ | $\kappa$ | 0.1464 | 0.1445 | 0.1430 | 0.1409 |
|---|---|---|---|---|---|
| $a^{-1} = 0.9176(93)$ GeV | $m_\pi/m_\rho$ | 0.547(4) | 0.694(2) | 0.753(1) | 0.807(1) |
| | $m_\pi^2$ GeV$^2$ | 0.238(1) | 0.571(1) | 0.814(1) | 1.128(1) |
| Fitting Range | | 10–18 | 12–18 | 12–20 | 12–20 |
| $\Delta\overline{E}_n^{\mathbf{P}}$ | [ $\times 10^{-3}$ GeV] | 22.5(34) | 13.2(12) | 11.42(70) | 8.78(40) |
| $\overline{p}_n^2$ | [ $\times 10^{-2}$ GeV$^2$] | 24.80(26) | 24.40(12) | 24.380(78) | 24.222(51) |
| $\delta(\overline{p}_n)$ | [degrees] | $-14.1(22)$ | $-10.7(10)$ | $-10.59(66)$ | $-9.25(43)$ |
| $A(m_\pi, \overline{p}_n)$ | | $-0.353(57)$ | $-0.348(33)$ | $-0.389(24)$ | $-0.387(18)$ |
| $\hat{A}(m_\pi, \overline{p}_n)$ | | $-1.06(17)$ | $-1.59(15)$ | $-2.34(14)$ | $-2.83(13)$ |
| $\beta = 1.95$ | $\kappa$ | 0.1410 | 0.1400 | 0.1390 | 0.1375 |
| $a^{-1} = 1.268(13)$ GeV | $m_\pi/m_\rho$ | 0.582(3) | 0.690(1) | 0.752(1) | 0.804(1) |
| | $m_\pi^2$ GeV$^2$ | 0.291(2) | 0.573(1) | 0.857(1) | 1.287(1) |
| Fitting Range | | 12–23 | 13–25 | 13–25 | 13–25 |
| $\Delta\overline{E}_n^{\mathbf{P}}$ | [ $\times 10^{-3}$ GeV] | 45.7(51) | 29.9(20) | 22.70(95) | 15.50(49) |
| $\overline{p}_n^2$ | [ $\times 10^{-2}$ GeV$^2$] | 27.55(30) | 27.02(14) | 26.761(79) | 26.389(48) |
| $\delta(\overline{p}_n)$ | [degrees] | $-20.9(24)$ | $-16.7(11)$ | $-14.63(63)$ | $-11.70(38)$ |
| $A(m_\pi, \overline{p}_n)$ | | $-0.549(68)$ | $-0.531(38)$ | $-0.535(23)$ | $-0.502(16)$ |
| $\hat{A}(m_\pi, \overline{p}_n)$ | | $-1.21(15)$ | $-1.67(12)$ | $-2.256(99)$ | $-2.787(91)$ |
| $\beta = 2.10$ | $\kappa$ | 0.1382 | 0.1374 | 0.1367 | 0.1357 |
| $a^{-1} = 1.833(22)$ GeV | $m_\pi/m_\rho$ | 0.576(3) | 0.691(3) | 0.755(2) | 0.806(1) |
| | $m_\pi^2$ GeV$^2$ | 0.291(1) | 0.605(2) | 0.896(1) | 1.332(2) |
| Fitting Range | | 18–35 | 18–35 | 18–35 | 18–35 |
| $\Delta\overline{E}_n^{\mathbf{P}}$ | [ $\times 10^{-3}$ GeV] | 58.8(69) | 44.1(25) | 34.6(14) | 26.80(78) |
| $\overline{p}_n^2$ | [ $\times 10^{-2}$ GeV$^2$] | 25.30(28) | 25.17(13) | 24.969(84) | 24.789(53) |
| $\delta(\overline{p}_n)$ | [degrees] | $-19.8(24)$ | $-18.7(11)$ | $-16.99(73)$ | $-15.44(46)$ |
| $A(m_\pi, \overline{p}_n)$ | | $-0.530(69)$ | $-0.626(39)$ | $-0.654(28)$ | $-0.697(21)$ |
| $\hat{A}(m_\pi, \overline{p}_n)$ | | $-0.90(11)$ | $-1.71(10)$ | $-2.29(10)$ | $-3.097(94)$ |

TABLE XIV. Results for $n = 0$ state in the laboratory system L1 with energy state cut-off $N = 3$. Two scattering amplitudes are defined by $A(m_\pi, \overline{p}_n) = \tan\delta(\overline{p}_n)/\overline{p}_n \cdot \overline{E}_n/2$ and $\hat{A}(m_\pi, \overline{p}_n) = (f_\pi^{lat}/f_\pi)^2 \cdot A(m_\pi, \overline{p}_n)$, where $f_\pi^{lat}$ is the pseudoscalar decay constant measured on lattice and $f_\pi = 93$ MeV.

| $\beta = 1.80$ | $\kappa$ | 0.1464 | 0.1445 | 0.1430 | 0.1409 |
|---|---|---|---|---|---|
| $a^{-1} = 0.9176(93)$ GeV | $m_\pi/m_\rho$ | 0.547(4) | 0.694(2) | 0.753(1) | 0.807(1) |
| | $m_\pi^2$ GeV$^2$ | 0.238(1) | 0.571(1) | 0.814(1) | 1.128(1) |
| Fitting Range | | 10–18 | 12–20 | 12–20 | 12–20 |
| $\Delta\overline{E}_n^{\mathbf{P}}$ | $[\times 10^{-3}$ GeV] | 9.5(10) | 6.72(50) | 4.65(43) | 3.70(19) |
| $\overline{p}_n^2$ | $[\times 10^{-3}$ GeV$^2$] | 54.16(69) | 58.93(46) | 59.04(45) | 59.56(23) |
| $\gamma$ | | 1.09436(62) | 1.04481(11) | 1.032523(71) | 1.024028(25) |
| $\delta(\overline{p}_n)$ | [degrees] | −7.03(76) | −7.14(52) | −5.81(52) | −5.36(27) |
| $A(m_\pi, \overline{p}_n)$ | | −0.286(30) | −0.409(28) | −0.391(34) | −0.419(20) |
| $\hat{A}(m_\pi, \overline{p}_n)$ | | −0.862(91) | −1.88(13) | −2.35(20) | −3.07(15) |
| $\beta = 1.95$ | $\kappa$ | 0.1410 | 0.1400 | 0.1390 | 0.1375 |
| $a^{-1} = 1.268(13)$ GeV | $m_\pi/m_\rho$ | 0.582(3) | 0.690(1) | 0.752(1) | 0.804(1) |
| | $m_\pi^2$ GeV$^2$ | 0.291(2) | 0.573(1) | 0.857(1) | 1.287(1) |
| Fitting Range | | 12–23 | 13–25 | 13–25 | 13–25 |
| $\Delta\overline{E}_n^{\mathbf{P}}$ | $[\times 10^{-3}$ GeV] | 17.3(11) | 11.99(55) | 9.62(35) | 6.92(30) |
| $\overline{p}_n^2$ | $[\times 10^{-3}$ GeV$^2$] | 61.40(58) | 64.47(36) | 65.73(28) | 65.91(28) |
| $\gamma$ | | 1.08447(51) | 1.04758(13) | 1.033120(56) | 1.022720(32) |
| $\delta(\overline{p}_n)$ | [degrees] | −9.29(59) | −8.55(38) | −8.20(29) | −7.12(30) |
| $A(m_\pi, \overline{p}_n)$ | | −0.392(24) | −0.473(20) | −0.540(18) | −0.566(23) |
| $\hat{A}(m_\pi, \overline{p}_n)$ | | −0.865(53) | −1.491(63) | −2.276(79) | −3.14(12) |
| $\beta = 2.10$ | $\kappa$ | 0.1382 | 0.1374 | 0.1367 | 0.1357 |
| $a^{-1} = 1.833(22)$ GeV | $m_\pi/m_\rho$ | 0.576(3) | 0.691(3) | 0.755(2) | 0.806(1) |
| | $m_\pi^2$ GeV$^2$ | 0.291(1) | 0.605(2) | 0.896(1) | 1.332(2) |
| Fitting Range | | 18–35 | 18–35 | 18–35 | 18–35 |
| $\Delta\overline{E}_n^{\mathbf{P}}$ | $[\times 10^{-3}$ GeV] | 27.8(12) | 17.7(65) | 14.75(48) | 10.45(38) |
| $\overline{p}_n^2$ | $[\times 10^{-3}$ GeV2] | 58.78(42) | 61.02(29) | 62.22(26) | 61.97(25) |
| $\gamma$ | | 1.07874(41) | 1.04214(13) | 1.029504(58) | 1.020373(39) |
| $\delta(\overline{p}_n)$ | [degrees] | −11.09(46) | −9.66(33) | −9.55(29) | −8.16(28) |
| $A(m_\pi, \overline{p}_n)$ | | −0.478(19) | −0.563(18) | −0.660(19) | −0.680(23) |
| $\hat{A}(m_\pi, \overline{p}_n)$ | | −0.816(32) | −1.544(50) | −2.311(68) | −3.02(10) |

TABLE XV. Results for $n = 1$ state in the laboratory system L1 with energy state cut-off $N = 3$. Two scattering amplitudes are defined by $A(m_\pi, \overline{p}_n) = \tan\delta(\overline{p}_n)/\overline{p}_n \cdot \overline{E}_n/2$ and $\hat{A}(m_\pi, \overline{p}_n) = (f_\pi^{lat}/f_\pi)^2 \cdot A(m_\pi, \overline{p}_n)$, where $f_\pi^{lat}$ is the pseudoscalar decay constant measured on lattice and $f_\pi = 93$ MeV.

| $\beta = 1.80$ | $\kappa$ | 0.1464 | 0.1445 | 0.1430 | 0.1409 |
|---|---|---|---|---|---|
| $a^{-1} = 0.9176(93)$ GeV | $m_\pi/m_\rho$ | 0.547(4) | 0.694(2) | 0.753(1) | 0.807(1) |
| | $m_\pi^2$ GeV$^2$ | 0.238(1) | 0.571(1) | 0.814(1) | 1.128(1) |
| Fitting Range | | 10–18 | 12–18 | 12–20 | 12–20 |
| $\Delta\overline{E}_n^{\mathbf{P}}$ | $[\times 10^{-3}$ GeV] | 28.0(63) | 18.1(26) | 14.6(12) | 10.62(59) |
| $\overline{p}_n^2$ | $[\times 10^{-2}$ GeV$^2$] | 30.65(53) | 30.41(27) | 30.31(14) | 30.061(79) |
| $\gamma$ | | 1.05169(54) | 1.03245(10) | 1.025510(52) | 1.020014(19) |
| $\delta(\overline{p}_n)$ | [degrees] | −16.9(39) | −13.4(20) | −12.1(10) | −9.86(56) |
| $A(m_\pi, \overline{p}_n)$ | | −0.405(98) | −0.406(61) | −0.412(35) | −0.379(21) |
| $\hat{A}(m_\pi, \overline{p}_n)$ | | −1.22(29) | −1.86(28) | −2.47(21) | −2.77(15) |
| $\beta = 1.95$ | $\kappa$ | 0.1410 | 0.1400 | 0.1390 | 0.1375 |
| $a^{-1} = 1.268(13)$ GeV | $m_\pi/m_\rho$ | 0.582(3) | 0.690(1) | 0.752(1) | 0.804(1) |
| | $m_\pi^2$ GeV$^2$ | 0.291(2) | 0.573(1) | 0.857(1) | 1.287(1) |
| Fitting Range | | 12–16 | 13–20 | 13–25 | 13–25 |
| $\Delta\overline{E}_n^{\mathbf{P}}$ | $[\times 10^{-3}$ GeV] | 57(10) | 34.0(37) | 28.3(16) | 18.98(79) |
| $\overline{p}_n^2$ | $[\times 10^{-2}$ GeV$^2$] | 34.21(67) | 33.30(28) | 33.26(14) | 32.788(81) |
| $\gamma$ | | 1.04789(53) | 1.03371(12) | 1.025787(45) | 1.019069(26) |
| $\delta(\overline{p}_n)$ | [degrees] | −25.0(47) | −17.3(19) | −16.35(99) | −12.59(53) |
| $A(m_\pi, \overline{p}_n)$ | | −0.63(13) | −0.516(60) | −0.555(34) | −0.495(21) |
| $\hat{A}(m_\pi, \overline{p}_n)$ | | −1.40(29) | −1.62(19) | −2.33(14) | −2.75(11) |
| $\beta = 2.10$ | $\kappa$ | 0.1382 | 0.1374 | 0.1367 | 0.1357 |
| $a^{-1} = 1.833(22)$ GeV | $m_\pi/m_\rho$ | 0.576(3) | 0.691(3) | 0.755(2) | 0.806(1) |
| | $m_\pi^2$ GeV | 0.291(1) | 0.605(2) | 0.896(1) | 1.332(2) |
| Fitting Range | | 18–22 | 18–35 | 18–35 | 18–35 |
| $\Delta\overline{E}_n^{\mathbf{P}}$ | $[\times 10^{-3}$ GeV] | 68(13) | 53.9(48) | 39.3(24) | 32.4(12) |
| $\overline{p}_n^2$ | $[\times 10^{-2}$ GeV$^2$] | 31.16(58) | 31.23(24) | 30.82(14) | 30.798(89) |
| $\gamma$ | | 1.04646(43) | 1.03077(10) | 1.023545(48) | 1.017343(30) |
| $\delta(\overline{p}_n)$ | [degrees] | −21.8(43) | −20.7(19) | −17.1(10) | −16.32(64) |
| $A(m_\pi, \overline{p}_n)$ | | −0.55(12) | −0.651(63) | −0.608(39) | −0.675(27) |
| $\hat{A}(m_\pi, \overline{p}_n)$ | | −0.95(20) | −1.78(17) | −2.13(13) | −3.00(12) |

TABLE XVI. Results for $n = 0$ state in the laboratory system L2 with energy state cut-off $N = 3$. Two scattering amplitudes are defined by $A(m_\pi, \overline{p}_n) = \tan\delta(\overline{p}_n)/\overline{p}_n \cdot \overline{E}_n/2$ and $\hat{A}(m_\pi, \overline{p}_n) = (f_\pi^{lat}/f_\pi)^2 \cdot A(m_\pi, \overline{p}_n)$, where $f_\pi^{lat}$ is the pseudoscalar decay constant measured on lattice and $f_\pi = 93$ MeV.

| $\beta = 1.80$ | $\kappa$ | 0.1464 | 0.1445 | 0.1430 | 0.1409 |
|---|---|---|---|---|---|
| $a^{-1} = 0.9176(93)$ GeV | $m_\pi/m_\rho$ | 0.547(4) | 0.694(2) | 0.753(1) | 0.807(1) |
| | $m_\pi^2$ GeV$^2$ | 0.238(1) | 0.571(1) | 0.814(1) | 1.128(1) |
| Fitting Range | | 10–18 | 12–18 | 12–18 | 12–20 |
| $\Delta\overline{E}_n^{\mathbf{P}}$ | $[\times 10^{-3}$ GeV$]$ | 7.2(21) | 4.79(84) | 3.81(50) | 2.03(27) |
| $\overline{p}_n^2$ | $[\times 10^{-2}$ GeV$^2]$ | 9.03(15) | 10.316(82) | 10.682(57) | 10.820(34) |
| $\gamma$ | | 1.1626(11) | 1.08224(20) | 1.06082(12) | 1.045678(45) |
| $\delta(\overline{p}_n)$ | [degrees] | −9.7(33) | −11.4(32) | −12.6(37) | −6.5(14) |
| $A(m_\pi, \overline{p}_n)$ | | −0.32(11) | −0.51(15) | −0.65(19) | −0.387(86) |
| $\hat{A}(m_\pi, \overline{p}_n)$ | | −0.98(34) | −2.37(69) | −3.9(11) | −2.83(63) |
| $\beta = 1.95$ | $\kappa$ | 0.1410 | 0.1400 | 0.1390 | 0.1375 |
| $a^{-1} = 1.268(13)$ GeV | $m_\pi/m_\rho$ | 0.582(3) | 0.690(1) | 0.752(1) | 0.804(1) |
| | $m_\pi^2$ GeV$^2$ | 0.291(2) | 0.573(1) | 0.857(1) | 1.287(1) |
| Fitting Range | | 12–16 | 13–20 | 13–25 | 13–25 |
| $\Delta\overline{E}_n^{\mathbf{P}}$ | $[\times 10^{-3}$ GeV$]$ | 15.5(25) | 7.5(10) | 5.49(71) | 3.12(37) |
| $\overline{p}_n^2$ | $[\times 10^{-2}$ GeV$^2]$ | 10.28(14) | 11.043(77) | 11.473(59) | 11.726(36) |
| $\gamma$ | | 1.14682(99) | 1.08709(25) | 1.06202(10) | 1.043336(60) |
| $\delta(\overline{p}_n)$ | [degrees] | −18.3(46) | −12.1(29) | −12.2(32) | −8.0(18) |
| $A(m_\pi, \overline{p}_n)$ | | −0.64(17) | −0.53(13) | −0.63(17) | −0.48(11) |
| $\hat{A}(m_\pi, \overline{p}_n)$ | | −1.42(38) | −1.69(41) | −2.66(73) | −2.70(62) |
| $\beta = 2.10$ | $\kappa$ | 0.1382 | 0.1374 | 0.1367 | 0.1357 |
| $a^{-1} = 1.833(22)$ GeV | $m_\pi/m_\rho$ | 0.576(3) | 0.691(3) | 0.755(2) | 0.806(1) |
| | $m_\pi^2$ GeV$^2$ | 0.291(1) | 0.605(2) | 0.896(1) | 1.332(2) |
| Fitting Range | | 18–30 | 18–35 | 18–35 | 18–35 |
| $\Delta\overline{E}_n^{\mathbf{P}}$ | $[\times 10^{-3}$ GeV$]$ | 17.5(35) | 9.3(15) | 7.83(88) | 4.45(61) |
| $\overline{p}_n^2$ | $[\times 10^{-2}$ GeV$^2]$ | 9.48(13) | 10.332(76) | 10.746(50) | 10.932(42) |
| $\gamma$ | | 1.13877(72) | 1.07789(27) | 1.05563(10) | 1.039047(74) |
| $\delta(\overline{p}_n)$ | [degrees] | −14.5(41) | −12.0(33) | −17.3(56) | −10.9(40) |
| $A(m_\pi, \overline{p}_n)$ | | −0.52(15) | −0.55(16) | −0.95(33) | −0.70(26) |
| $\hat{A}(m_\pi, \overline{p}_n)$ | | −0.89(26) | −1.53(44) | −3.3(11) | −3.1(11) |

TABLE XVII.　Results for $n = 1$ state in the laboratory system L2 with energy state cut-off $N = 3$. Two scattering amplitudes are defined by $A(m_\pi, \overline{p}_n) = \tan\delta(\overline{p}_n)/\overline{p}_n \cdot \overline{E}_n/2$ and $\hat{A}(m_\pi, \overline{p}_n) = (f_\pi^{lat}/f_\pi)^2 \cdot A(m_\pi, \overline{p}_n)$, where $f_\pi^{lat}$ is the pseudoscalar decay constant measured on lattice and $f_\pi = 93$ MeV.

| $\beta = 1.80$ | $\kappa$ | 0.1464 | 0.1445 | 0.1430 | 0.1409 |
|---|---|---|---|---|---|
| $a^{-1} = 0.9176(93)$ GeV | $m_\pi/m_\rho$ | 0.547(4) | 0.694(2) | 0.753(1) | 0.807(1) |
| | $m_\pi^2$ GeV$^2$ | 0.238(1) | 0.571(1) | 0.814(1) | 1.128(1) |
| Fitting Range | | 10–18 | 12–18 | 12–20 | 12–20 |
| $\Delta\overline{E}_n^{\mathbf{P}}$ | [ $\times 10^{-3}$ GeV] | 9.5(18) | 6.80(73) | 5.38(44) | 4.47(24) |
| $\overline{p}_n^2$ | [ $\times 10^{-2}$ GeV$^2$] | 12.26(13) | 12.217(71) | 12.152(49) | 12.120(30) |
| $\gamma$ | | 1.14900(84) | 1.08007(19) | 1.05990(11) | 1.045213(44) |
| $\delta(\overline{p}_n)$ | [degrees] | −11.3(18) | −9.36(82) | −8.12(54) | −7.35(32) |
| $A(m_\pi, \overline{p}_n)$ | | −0.345(55) | −0.393(34) | −0.396(26) | −0.414(17) |
| $\hat{A}(m_\pi, \overline{p}_n)$ | | −1.03(16) | −1.80(15) | −2.37(15) | −3.03(13) |
| $\beta = 1.95$ | $\kappa$ | 0.1410 | 0.1400 | 0.1390 | 0.1375 |
| $a^{-1} = 1.268(13)$ GeV | $m_\pi/m_\rho$ | 0.582(3) | 0.690(1) | 0.752(1) | 0.804(1) |
| | $m_\pi^2$ GeV$^2$ | 0.291(2) | 0.573(1) | 0.857(1) | 1.287(1) |
| Fitting Range | | 12–16 | 13–25 | 13–25 | 13–25 |
| $\Delta\overline{E}_n^{\mathbf{P}}$ | [ $\times 10^{-3}$ GeV] | 18.2(26) | 13.6(11) | 10.81(61) | 8.71(41) |
| $\overline{p}_n^2$ | [ $\times 10^{-2}$ GeV$^2$] | 13.49(15) | 13.415(83) | 13.333(51) | 13.288(40) |
| $\gamma$ | | 1.13642(69) | 1.08428(22) | 1.060890(97) | 1.042870(58) |
| $\delta(\overline{p}_n)$ | [degrees] | −14.4(16) | −12.20(83) | −10.63(48) | −9.51(36) |
| $A(m_\pi, \overline{p}_n)$ | | −0.459(53) | −0.496(33) | −0.511(23) | −0.547(20) |
| $\hat{A}(m_\pi, \overline{p}_n)$ | | −1.01(11) | −1.56(10) | −2.156(98) | −3.04(11) |
| $\beta = 2.10$ | $\kappa$ | 0.1382 | 0.1374 | 0.1367 | 0.1357 |
| $a^{-1} = 1.833(22)$ GeV | $m_\pi/m_\rho$ | 0.576(3) | 0.691(3) | 0.755(2) | 0.806(1) |
| | $m_\pi^2$ GeV$^2$ | 0.291(1) | 0.605(2) | 0.896(1) | 1.332(2) |
| Fitting Range | | 18–30 | 18–35 | 18–35 | 18–35 |
| $\Delta\overline{E}_n^{\mathbf{P}}$ | [ $\times 10^{-3}$ GeV] | 31.5(32) | 21.2(12) | 17.99(92) | 15.12(66) |
| $\overline{p}_n^2$ | [ $\times 10^{-2}$ GeV2] | 12.72(13) | 12.542(63) | 12.522(53) | 12.511(45) |
| $\gamma$ | | 1.12865(64) | 1.07562(21) | 1.05469(10) | 1.038631(69) |
| $\delta(\overline{p}_n)$ | [degrees] | −17.4(14) | −13.61(65) | −12.56(52) | −11.68(42) |
| $A(m_\pi, \overline{p}_n)$ | | −0.568(48) | −0.584(27) | −0.636(26) | −0.705(24) |
| $\hat{A}(m_\pi, \overline{p}_n)$ | | −0.969(81) | −1.603(75) | −2.226(91) | −3.13(11) |

[1] S. R. Sharpe, R. Gupta, and G.W. Kilcup, Nucl. Phys. **B383**, 309 (1992).

[2] R. Gupta, A. Patel, and S. R. Sharpe, Phys. Rev. D **48**, 388 (1993).

[3] Y. Kuramashi, M. Fukugita, H. Miho, M. Okawa, and A. Ukawa, Phys. Rev. Lett. **71**, 2387 (1993); M. Fukugita, Y. Kuramashi, M. Okawa, H. Miho, and A. Ukawa, Phys. Rev. D **52**, 3003 (1995).

[4] M. G. Alford and R. L. Jaffe, Nucl. Phys. **B578**, 367 (2000).

[5] BGR Collaboration, K. J. Juge *et al.*, Nucl. Phys. B, Proc. Suppl. **129**, 194 (2004).

[6] JLQCD Collaboration, S. Aoki *et al.*, Phys. Rev. D **66**, 077501 (2002).

[7] C. Liu, J. Zhang, Y. Chen, and J. P. Ma, Nucl. Phys. **B624**, 360 (2002).

[8] CP-PACS Collaboration, A. Ali Khan *et al.*, Phys. Rev. D **67**, 014502 (2003).

[9] H. R. Fiebig, K. Rabitsch, H. Markum, and A. Mihàly, Few-Body Syst. **29**, 95 (2000).

[10] M. Lüscher, Commun. Math. Phys. **105**, 153 (1986).

[11] M. Lüscher, Nucl. Phys. **B354**, 531 (1991).

[12] M. Lüscher and U. Wolff, Nucl. Phys. **B339**, 222 (1990).

[13] C. Kim, Nucl. Phys. B, Proc. Suppl. **129**, 197 (2004).

[14] C. Bernard and M. Golterman, Phys. Rev. D **53**, 476 (1998).

[15] G. Colangelo and E. Pallante, Nucl. Phys. **B520**, 433 (1998).

[16] CP-PACS Collaboration, S. Aoki *et al.*, Phys. Rev. Lett. **85**, 4674 (2000); **90**, 029902(E) (2003); Phys. Rev. D **65**, 054505 (2002); **67**, 059901(E) (2003).

[17] K. Rummukainen and S. Gottlieb, Nucl. Phys. **450**, 397 (1995).

[18] Y. Iwasaki, Nucl. Phys. **B258**, 141 (1985); University of Tsukuba Report No. UTHEP-118, 1983 (to be published).

[19] B. Sheikholeslami and R. Wohlert, Nucl. Phys. **B259**, 572 (1985).

[20] J. Gasser and H. Leutwyler, Annals Phys. **158**, 142 (1984).

[21] G. Rupak and N. Shoresh, Phys. Rev. D **66**, 054503 (2002); O. Bär, G. Rupak, and N. Shoresch, hep-lat/0306021; S. Aoki, Phys. Rev. D **68**, 054508 (2003).

[22] N. Kawamoto and J. Smit, Nucl. Phys. **B192**, 100 (1981).

[23] G. Colangelo, J. Gasser, and H. Leutwyler, Nucl. Phys. **B603**, 125 (2001).

[24] W. Hoogland *et al.*, Nucl. Phys. **B126**, 109 (1977).

[25] M. J. Losty *et al.*, Nucl. Phys. **B69**, 185 (1974).

[26] X. Li and C. Liu, Phys. Lett. **B587**, 100 (2004).